CHAPTER 1

INTRODUCTION

1.1 GENERAL

The digital image processing deals with developing a digital system that performs operations on a digital image. The digital image analysis is a smart tool with deferential capabilities for analyzing the intrinsic micro-structural features and extract necessary and relevant information like size, shape and orientation, the relative distribution of pores and particles with the desired accuracy. The digital image processing is widely used for exploring and understanding the various materials in material science such as porous media, metals and alloys, fibrous materials, composites, catalyst, polymers; in electronics such as semi-conductors and life science such as cellular biology and structural biology for numerous microstructural characterization studies. In civil engineering, recently image processing techniques have been used widely for characterization of the geomaterials such as rocks in oil and gas industry, soils, geotextiles, etc. Thus, due to rapid technological development in the field of computer and softwares the scope of research has increased. It has led to faster and more accurate results generation.

One of the major objective in geotechnical engineering is to obtain the properties of in situ soil in order to evaluate its various mechanical properties such as permeability, strength, stiffness and bearing capacity. The various tests conducted and the data obtained from them are highly subjective which makes the evaluation of these tests with varying soil conditions over space and time extremely challenging. In order to get precise results, method of characterization of soils should be versatile and automated.

The sand is employed for numerous applications in the civil engineering field; particularly as a raw material for constructing high rise buildings, infrastructure, shallow and deep foundations, earthen dams, embankments and backfills as well as filtration and drainage applications. Its performance value depends primarily on important properties such as porosity, particle size distribution, pore size distribution, permeability etc. Yet, conventional and standard methods followed for determining these properties lack universal acceptance, due to limitations such as high operator dependence, non-repeatability of results and most importantly, huge time consumption.

In view of this, present study aims to develop a more reliable method of microstructural characterization of soil with the help of digital image processing. In the study, soil specimen preparation technique using resin impregnation method was adopted so that an observation surface will be produced after cutting of the specimen, which will be thereafter used for high quality image acquisition. Further, the study will evaluate the microstructural properties of commercially available Indian grade II sand (0.5-1 mm) such as porosity, pore size distribution and particle size distribution using different image processing softwares. The results from these softwares will be compared in order to conclude the better image processing software. The second part of the study was to develop an innovative method of finding the air permeability of glass beads using digital pressure sensor and data logger. This method was found to be more accurate, reliable, versatile than conventional methods. Ultimately, both the studies have used the automation, so that the results are precise, reliable and versatile.

1.2 OBJECTIVE AND SCOPE

The objective of the study is to perform analysis of the digital image captured using digital single lens reflex camera and processed with the help of Image J and Avizo fire software. In view of this, the scope of the work involves the following:

1. Developing a resin impregnation method for preparing a sand specimen for microstructural analysis.
2. Critical analysis of digital image captured using digital single lens reflex camera and processed using Image J and Avizo fire for finding pore size properties of sand
3. Development of an experimental apparatus to measure air permeability and hydraulic conductivity for glass beads simultaneously and further can be subjected to the resin impregnation technique.
4. Literature review for applications of lightweight cellular cemented clay in geotechnical engineering and process involved in manufacturing.

1.3 ORGANISATION OF THESIS

The thesis contains a total of seven chapters based on the research carried out. Chapter 1 shows the importance of digital image processing in geotechnical engineering. Chapter 2 presents the

review of the various techniques as well as the fundamental process involved in the digital image processing to evaluate micro level properties of soils. The basic concepts and definitions of porosity, pore size distribution and particle size distribution have been discussed. Later, the importance of air permeability have been discussed. Various existing predictive models of permeability have been discussed. Chapter 3 deals entirely with respect to lightweight cellular cemented clay. Various applications of lightweight cellular cemented clay as an innovative material have been reviewed and the steps involved in the manufacturing of lightweight cellular cemented clay have been discussed.

Chapter 4 explains the development of methodology for digital image processing, hydraulic conductivity and air permeability experiments. The newly fabricated experimental apparatus have been discussed in detail. Chapter 5 summarizes the results of the experimental work of digital image processing, hydraulic conductivity, air permeability and discusses the results in detail. Chapter 6 reports the concluding remarks of study along with the future scope of the work.

CHAPTER 2

LITERATURE REVIEW

2.1 DIGITAL IMAGE ANALYSIS

A digital image is a representation of a two-dimensional image using ones and zeros (binary). It provides discrete values.The digital image processing deals with developing a digital system that performs operations on a digital image. Due to the rapid advancement in the field of science and technology, the use of computers and automated digital image processing has widely developed (Doktor et al., 2010, Doktor et al., 2011). Digital image processing has been used by researchers such as Sardini et al. (2009), to map the pore distribution in rocks.The digital image analysis is a smart tool with deferential capabilities for analyzing the intrinsic micro-structural features and extract necessary and relevant information like size, shape and orientation, the relative distribution of pores and particles with the desired accuracy.

In the experiment conducted, digital image analysis was used as a technique for the analysis of images captured. Digital image analysis can be used for finding the micro-structural properties of soil. There are various types of digital image acquisition techniques such as X-ray computed tomography, scanning electron microscope and digital camera. Elliot et al. (2007) showed X-ray CT technique has been used for void analysis in thin soil section. Image acquisition can also be performed by X-ray computed tomography as well as scanning electron microscope (SEM) as shown by Doktor et al., (2010). Rozenbaumet al. (2012) showed the porosity resulting from assemblage of the silt-clay from the X-ray CT. There are various drawbacks associated with X-ray computed tomography and scanning electron microscope such as non-reliability, difficult to use and expensive instruments.In order to tackle this problem, digital camera was seen as a viable option for image acquisition due to the following reasons:

1. Better quality images can be captured
2. Ease of using
3. Affordable as compared to X-computed tomography, scanning electron microscopeinstruments
4. Reliablei.e. can be used anywhere and anytime.

Hence, it can be seen that digital camera has large number of advantages over X-CT and SEM. Digital camera was used for image acquisition in the experiment conducted. For the processing of the image, Image J and Avizo fire image processing software were used.

Image J is public domain, Java based image processing program which was developed by Wayne Rasband at National Institutes of Health. The version used was 1.49. ImageJ is the world's fastest pure Java image processing program. Image J can read many image file formats such as TIFF, PNG, GIF, JPEG, BMP, DICOM and FITS. In the image enhancement part, it supports smoothing, sharpening, edge detection, filtering and thresholding on both 8-bit grayscale and RGB color images and can also adjust brightness and contrast of 8, 16 and 32-bit images. In the analysis part, it can measure area, mean, standard deviation, min and max of selection or entire image, measure lengths and angles. It can be used with real world measurement units such as millimeters. It can generate histograms and profile plots.

Avizo fire is an image analysis software package designed to work smoothly with 3D images and also 2D image. Avizo has been designed to support different types of applications and workflows from 2D and 3D image data processing to simulations. It is a versatile and customizable visualization tool used in many fields.

Fundamental steps in image processing:

1. **Image acquisition:** It deals with acquiring a digital image using any one of the image capturing method.

2. **Image conversion:** It converts the input data to a form suitable for computer processing.

3. **Image enhancement:** The idea behind enhancement techniques is to bring out details that are hidden, or simply to highlight certain features of interest in an image such as, changing brightness & contrast etc.

4. **Image thresholding:** The simplest thresholding methods replace each pixel in an image with a black pixel if the image intensity is less than some fixed constant or a white pixel if the image intensity is greater than that constant. This image can be converted into binary image of black and white if the thresholding is performed in RGB (red-green-blue) colours.

5. **Morphological operation:** It is much easier to perform morphological operations on binary image. It deals with tools for extracting image components that are useful in the representation and description of shape.

6. **Image segmentation:** It is used to make partitions into an input image into its constituent parts or objects. Many softwares use water shed segmentation for partition image into its constituent parts or objects. The water shed segmentation considers the gradient magnitude of an image as a topographic surface. Pixels having the highest gradient magnitude intensities (GMIs) correspond to watershed lines, which represent the region boundaries. Water placed on any pixel enclosed by a common watershed line flows downhill to a common local intensity minimum (LIM). Pixels draining to a common minimum form a catch basin, which represents a segment.A rugged segmentation procedure brings the process a long way toward successful solution of imaging problems that require objects to be identified individually.On the other hand weak or erratic segmentation algorithms almost always guarantee eventual failure. In general, the more accurate the segmentation, the more likely recognition is to succeed.

7. **Image representation:** It almost follows the output of the segmentation stage. In this, a representation has to be chosen for the data either as outlines, masked, etc. Boundary representation is appropriate when the focus is on is on external shape characteristics such as corners and inflections. Regional representation is appropriate when the focus is on internal properties such as texture or skeletal shape. Choosing a representation is only part of the solution for transforming raw data into a suitable for subsequent computer processing.

8. **Image description:** It deals with extracting attributes that result in some quantitative information of interest or are basic for differentiating one class of objects from another.The results are generated after performing the above steps.
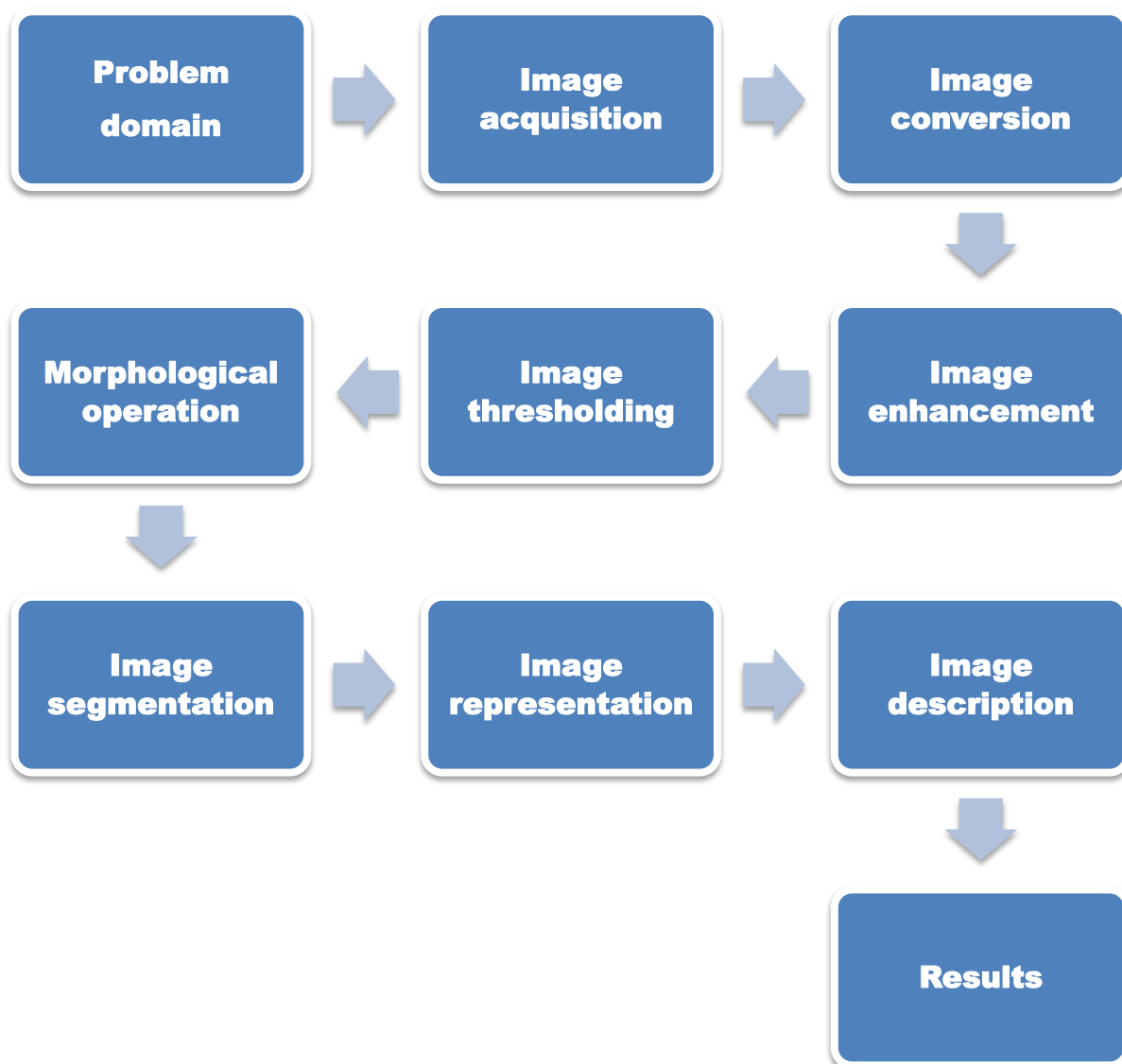
Fig. 2.1 Steps involved in digital image processing

2.2 PROPERTIES RELATED TO POROUS MEDIA

Pore size distribution, PSD is one of the most important parameter of the soil. The basic character of the PSD affects and is affected by critical aspects of almost everything that occurs in the soil: the movement of water, air, and other fluids; the transport and the reaction of chemicals; and the residence of roots and other biological organisms. Pore characteristics are related to particle size characteristics. A large amount of research in particle size characteristics is present but research in pore size characteristics is lesser than particle size characteristics. Hence, pore size characteristics have been discussed in order to relate to permeability.

The pore space is often considered in terms of individual pores an artificial concept that enables quantifications of its essential character. Pore size distribution plays an important role in defining the various properties of coarse-grained soils. A proper understanding of pore structure is essential in many areas of geotechnical engineering where fluid transport is involved. The significant influence of various microstructural properties such as total and effective porosities; pore size distribution and the fundamental properties such as shear strength, permeability, and compressibility of soils has been well recognized by the geotechnical engineering fraternity (Czupak, 2011).

Apart from pore size distribution, total and effective porosity also affect the fundamental behavior of the soil under various conditions. Effective porosity is that portion of the total void space of a porous material that is capable of transmitting a fluid. Total porosity is the ratio of the total void volume to the total bulk volume.

2.2.1 *Porosity*

The basic definition of porosity is a ratio of void space to total volume.This definition deals with 3D porosity. The 2D porosity is the summed area of pore space divided by total area which is also called as the areal porosity over that plane. Kovacs (1981) showed that the areal porosity is equal to volumetric porosity for randomly distributed pores. It is a single-value quantification of the amount of space available to fluid within a specific body of soil. Being simply a fraction of total volume, porosity can range between 0 and 1, typically falling between 0.3 and 0.7 for soils

The porosity of a soil depends on several factors, including

1. Packing density of soil
2. Shape of particles of soil
3. Cementing in soil
4. Arrangement of particles of soil

In unconsolidated materials, the porosity depends on packing, shape and arrangement. In consolidated materials, compaction, cementation and consolidation are important as they vary with depth, porosity will also vary accordingly. Graton and Fraser (1935) analysed the porosity of various packing arrangements of uniform spheres. The least compact arrangement of uniform

spheres is that of cubical packing (Fig. 2.2a) with a porosity of 47.6 %. The most compact packing of uniform spheres is rhombohedral (Fig. 2.2b) one, in which porosity is 25.96 %. Mathematically considering an idealized soil of packed uniform spheres, porosity must fall between 0.26 and 0.48, depending on the packing.

For a specific packing, porosity of spherical objects is same for different size of the grains. This means if we have any two sizes of spherical objects having similar packing and arrangement, then its porosity is the same. The particles stacked directly on top of each other (cubic packing) have higher porosity than the particles in a pyramid shape sitting on top of two other particles (rhombohedral packing) as shown in Fig. 2.2a and 2.2b. Generally, a mixture of grain sizes and shapes results in lower porosity.
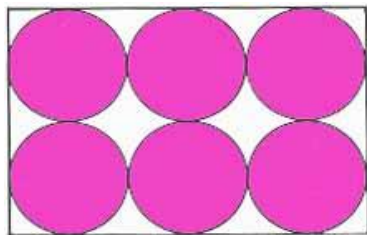
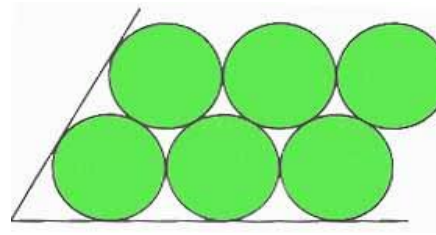**Fig. 2.2a Cubic packing of spherical particles (porosity= 47.6 %)**   **Fig. 2.2b Rhombohedral Packing of spherical particles (porosity = 25.96 %)**

2.2.2 *Pore Size*

Defining pore size is one of the complex topics because the soil does not contain discrete objects with obvious boundaries that could be called individual pores, the precise delineation of a pore unavoidably requires artificial, subjectively established distinctions. This contrasts with soil particles, which are easily defined, being discrete material objects with obvious boundaries. The arbitrary criterion required to partition pore space into individual pores is often not explicitly stated when pores or their sizes are discussed (Nimmo, 2004).In this study, pore size has been defined for 2D structure. Defining pore size of 2D structure is much simpler than 3D soil structure.

There are two of definitions of pore size that were found out in the study for 2D soil structure. Defining a "pore size" is by defining a pore diameter at a point within the pore space of a porous medium as the diameter of the largest sphere that contains this point while still remaining

9

entirely within the pore space (Bear, 1972). In other words, it is the largest spherical diameter particle that can pass through a single pore. Alternatively, image analysis software such as Image J, Avizo fire gives pore area rather than pore diameter. This pore area can be converted into an equivalent diameter. Hence, latter is better and easy method.

Pore bodies are the relatively wide portions and pore openings are the relatively narrow portions that separate the pore bodies. Other anatomical metaphors are sometimes used, the wide part of a pore being the "belly" or "waist", and the constructive part being the "neck" or "throat" (Nimmo, 2004). Pore sizes are usually specified as the diameter of the pore body.

2.2.3 *Pore size distribution*

The importance of a soil's pore size distribution is that it relates to other soil properties in a complex and useful way. It indicates complexity of structure in far more detail than porosity alone. The spatial variation of pore size is an important characteristic of the medium. The relation of pore size to particle size distribution in a randomly structured medium is likely to be monotone: larger pores are associated with larger particles. The non-random structure of most soils adds complexity to the relation between pore size and particle size. Large pores can be associated not only with large particles, but also with smaller particles such as clays that promote aggregation and hence the existence of large inter-aggregate pores.

While these distributions can be described by an average diameter value, it will hardly reveal any information concerning the shape of the distribution curve. For this reason, the distribution curves generated by the mercury intrusion and capillary flow porosity instruments should be considered in their entirety and not simplified to a single value. Also, note the various pore size distributions that can be created from different material geometries. Fig. 2.2c shows an example in which one graph represents pore-opening and pore-body size distributions. Portions of the $f(r)$ area are shaded differently, based on criteria of how the pore body radius (r_w in this diagram) relates to the pore opening radius (r_d in this diagram) and to r_s (defined on the abscissa).
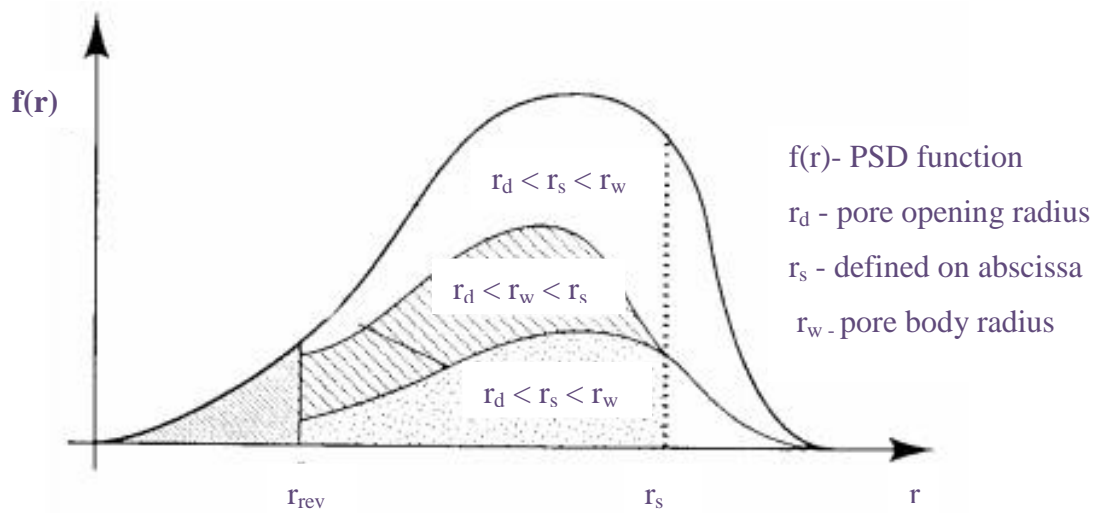
Fig. 2.2c Hypothetical pore size distribution with sub-regions distinguished on the basis of pore body and opening radii and drying/wetting history (Nimmo, 2004)

Defining the pore size distribution using a single value is limiting as different pore sizes are present in thesoil. Hence, pore size distribution should be represented graphically rather than a single value. Many studied have shown that pore size distribution can be assumed to be a normal distribution curve.The distribution curve can be described in more detail by evaluating the upper limit, lower limit, mean and standard deviation of the normal distribution curve. It can be represented by a function f(r), which has a value proportional to the combined volume of all pores whose effective radius is within an infinitesimal range centered on r.

Meyer (1999) expressed pore size distribution in the form of pore volume distribution depending on pore radius. Nimmo (2004) expressed that often a specific functional model such as log-normal or normal distribution can fit the pore size data. In the study, pore size distribution will be expressed in the form of pore area distribution depending on the pore diameter.

2.2.4 *Conventional Methodologies*

The conventional methods for determination of pore size distribution of soils include gas adsorption, mercury intrusion porosimetry (MIP), capillary condensation/non-polar liquid sorption and thin section techniques (Diamond, 1970; Lawrence, 2006).Mercury intrusion porosimetry is the traditional method for pore characterization of fine-grained particles. Among the various techniques available for observing the pore size distribution of soil fabric, MIP is

11

observed to be more objective, repeatable and quantitative. The limitations of the conventional methods include expensive equipment, non-reliability and difficulty in use.

2.3 PERMEABILITY

Air permeability of soil (and other porous materials) is the coefficient, K_{air} governing the convective transmission of air through soil under an applied total pressure gradient. It is also called as intrinsic permeability. The unit of intrinsic permeability is square meters. Intrinsic permeability is related to the nature of porous medium hence is constant for different fluid properties. Hence, $K_{air} = K_{water}$ for a given porous medium. The intrinsic permeability and hydraulic conductivity of porous medium are related as shown in following equation:

$$k = (K \times \rho \times g)/\mu \qquad (1)$$

k = hydraulic conductivity (m/s)

K = intrinsic permeability for a given porous medium(m^2)

ρ = density of the fluid, kg/m^3

μ = dynamic viscosity (Pa.s)

g = acceleration due to gravity (m/s^2)

The factors that control the permeability of a soil are as follows:

- **Geometry of the porous network**

  Permeability varies with the square of particle diameter. It is logical that the smaller the grain-size, the smaller the voids and the lower the permeability. A relationship between permeability and grain-size is more appropriate in case of sands and silts than that in case of other soils since the grains are more equidimensional and its fabric changes are not significant. This suggests a simple method for assessment of permeability of a soil at any void ratio when values of permeability are known at two or more void ratios. Once the line is drawn, permeability at any void ratio may be read directly.

- **Composition**

  Influence of soil composition on permeability is generally of little significance in case of gravels, sands, and silts, unless mica and organic matters are present. However, this is of major importance in the case of clays. Montmorillonite has the least permeability with

sodium as the exchangeable ion (less than 10^{-7} cm/s). Therefore, sodium montmorillonite is used by the engineer as an additive to other soils to make them impermeable. Kaolinite is hundred times more permeable than montmorillonite.

- **Fabric or arrangement of particles**

  Fabric or structural arrangement of particles is an important soil characteristic influencing permeability, especially of fine-grained soils. At the same void ratio, it is logical to expect that a soil in the most flocculated state will have the highest permeability and the one in the most dispersed state will have the lowest permeability. Remolding of a natural soil invariably reduces its permeability. Stratification or macrostructure also has great influence on the permeability, it is more parallel to stratification than that perpendicular to stratification.

- **Properties of the permeating fluid (viz., viscosity and density)**

  The high viscosity of the fluid will give low permeability. An inverse relation is present between permeability and viscosity

- **Degree of saturation**

  Higher the degree of saturation, higher the permeability. In case of certain sands permeability may increase three-fold when degree of saturation increases from 80% to 100%.

- **Presence of entrapped air and other foreign matter**

  Entrapped air has pronounced effect on permeability. It reduces the permeability of soil. Organic foreign matter also has the tendency to move towards flow channels and choke them, thus decreasing the permeability. Natural soil deposits in the field may have some entrapped air or gas for several reasons. In the laboratory, air-free distilled water may be used as vacuum applied to achieve a high degree of saturation. However, this may not lead to a realistic estimate of the permeability of a natural soil deposit.

Because pores are fluid conduits, their size distribution is useful for predicting permeability k. The size of pore space and interconnectivity of the pore spaces will help determine permeability. Interconnectivity of pores is a function of the shape of the particle (sphericity) and tortuosity of the porous medium. Hence, larger the pore space and interconnectivity mean greater permeability of the material. Various predictive equations based on volumetric and grain size parameters have been proposed to estimate the permeability. These predictive equations have

had limited success for coarser soils but have been completely unsatisfactory for fine-grained soil. The following table shows the hydraulic conductivity of different soils.

Table 2.3 Hydraulic conductivity of different soils (C.W. Fetter, 1994)

Material	Hydraulic Conductivity (m/s)
well-sorted gravel	10^{-4} to 0.01
well-sorted sands	10^{-5} to 10^{-3}
fine sands	10^{-7} to 10^{-5}
silt, sandy silts, clayey sands	10^{-8} to 10^{-6}
clay	10^{-11} to 10^{-8}

2.3.1 *Predictive models of permeability*

There is no engineering soil property that can vary more widely than that of the coefficient of permeability. For saturated soil, the coefficient of permeability can vary more than 10 orders of magnitude when considering the soils that range from a gravel to a clay. This wide range in the coefficient of permeability has proven to be a major obstacle in analyzing seepage problems. Based on the literature review conducted, the following equations were found to correlate permeability and particle/pore size.

Hazen's equation:

Hazen's equation is the most common correlation equation used to estimate coefficient of permeability for sands.Allen Hazen (1892) showed that permeability is directly proportional to the square of a diameter that which 10% by weight of soil grains are finer. He also showed direct proportionality to thesquare of pore diameter for sands.

$$K \text{ } \alpha \text{ pore size} \sim (\text{pore diameter})^2, \text{ pore diameter} \sim D_{10}$$

$$k = C \times D_{10}^2 \qquad (2)$$

k = coefficient of permeability (cm/sec)

C = constant (typically 1, range is 0.4 to 1.2)

D_{10} = 10% finer diameter of particles mm (0.1 mm < D_{10} < 3 mm)

Kozeny - Carman equation:

Another empirical equation for predicting permeability from grain size distribution, originally proposed by Kozeny (1927) and modified by Carman (1937, 1956), to become the Kozeny-Carman equation. This equation was developed after considering a porous material as an assembly of thecapillary tube. In the geotechnical literature, there is a large consensus that the Kozeny-Carman (KC) equation applies to sands but not to clays. Such opinion, however, is supported only by partial demonstration. Since its first appearance (Carman 1937) to the present, this equation has taken several forms, including the following one that is commonly used:

The KC equation relates the permeability K and porosity $\eta$by Carman PC (1939)

$$K \;=\; 1/\,(c \times S^2) \times \eta^3/(1-\eta)^2 \tag{3}$$

where$c$ and S denote Kozeny constant and specific surfacearea based on the solid volume, respectively.After including the tortuosity factor (T),which is the ratio of the length of the curve (L_t) to the distance between the ends of it (L_0); the KC equation can be further modified as Bear (1972)

$$K \;=\; 1/(36 \times k) \times \eta^3/(1-\eta)^2 \times d^2 \tag{4}$$

where K = intrinsic permeability, $k \;=\; cT^2$ is the KC constant, $T \;=\; L_t/L_0$ is the tortuosityand $d \;=\; 6/S$ is the mean diameter of the hypotheticalspherical solid particles with the same specific surface area S. $T$is approximated by $\sqrt{2}$and c is taken to be about 2.5 for beds packed withspherical particles, then the empirical KC constant $(k \;=\; cT^2)$ is approximated to be 5.

$$k \;=\; 1/\,(C_s \times S^2 \times T^2) \;\times\; (\gamma_w/\,\mu) \times \eta^3/(1-\eta)^2 \tag{5}$$

where k = coefficient of permeability, C_s = shape factor, μ= dynamic viscosity of water.It yielded the coefficient of permeability k as a function of the porosity η (or void ratio e), the specific surface S(m^2/kg of solids) and a factor C_s to take into account the shape and tortuosity of channels. In practice, this equation with the specific surface area is not frequently used. The reason seems to lie in the difficulty to determine the soil specific surface. Hence, the Eq. 4

should be used instead of Eq. 5, as Eq. 4 shows dependency of permeability on the diameter of the particles.

Taylor relationship:

In soil mechanics, Taylor (1948) illustrated the linear relationship between k and $e^3/(1 + e)$. He registered also a good correlation between k and e^2. Later, it was shown that plot of $e^3/(1 + e)$ versus k and plot of $\log k$ versus e also shows a straight line within a range of permeability values. Thus, we can get permeability of a soil at any void ratio when values of permeability are known at two or more void ratios. After drawing the line, the permeability at any void ratio can be read directly.

Krumbein and Monk's equation:

Krumbein and Monk (1942) measured permeability in sand packs of constant 40% porosity for specified size and sorting ranges. Analysis of their data, coupled with dimensional analysis of the definition of permeability, led to

$$K = 760 \times d_g^2 \times exp(-1.31\sigma_D) \tag{6}$$

where K is given in darcies (1 darcy = 9.97E-13 m^2)

d_g is the geometric mean grain diameter (mm)

σ_D is the standard deviation of grain diameter in ϕ units, where $\phi = -\log_2(d)$ and d is expressed in millimetres. Although the Krumbein and Monk equation is based on sand packs of 40% porosity and does not include porosity as a parameter. He concluded that normal or log-normal distribution of grain size distribution can be used in the estimation of permeability.

2.3.2 *Air permeability*

Air flow plays an important role in geotechnical engineering, especially in unsaturated soils. Determination of air permeability of unsaturated porous materials is an important parameter in the understanding of vapour phase contaminant migration. There are large numbers of applications of air flow in soils. Removal of hazardous volatile soil contaminants and removal of methane in landfills are some of the applications where air flow property or air permeability is required (U. S. EPA, 2012).

There are two common methods that are useful in the removal of hazardous volatile soil contaminants. The first one is soil vapour extraction and the other one is air sparging. Vapours are the gases that form when chemicals evaporate. Soil vapour extraction extracts vapours from the soil above the water table by applying a vacuum to evacuate the vapours out. Air sparging, on the other hand, pumps air underground to help extract vapours from groundwater and wet soil found beneath the water table. Extracted air and contaminant vapours, sometimes referred to as "off-gases," are treated to remove any harmful levels of contaminants using activated carbon, bio-filtration or heating them to high temperatures. Fig. 2.3 shows theair sparging and soil vapour extraction methods.
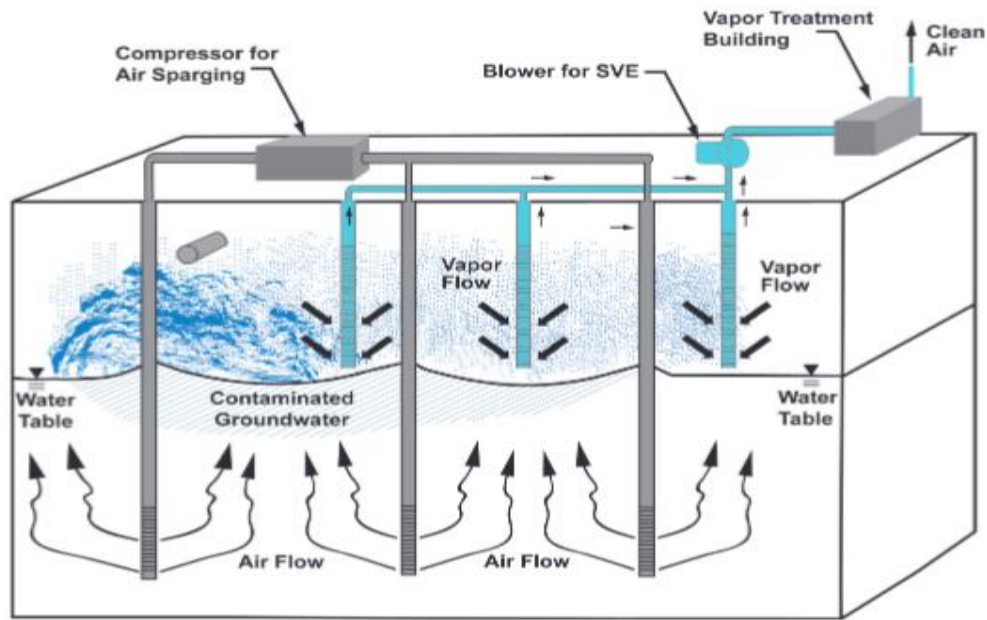
Fig. 2.3 Illustration on air sparging and soil vapour extraction (U.S. EPA, 2012)

Darcy's law and Fick's law (diffusion) can be used to describe the flow of air through a porous medium. But Fick's law is not applicable when the porous medium has zero water content. Hence, Darcy's law should be applied to calculate air permeability. The basic physical conditions include a Darcian flow regime, one dimensional, incompressible fluids, steady state conditions, isothermal and laminar flow of a viscous gas. Darcy's equation is shown as follows:

$$K_a = [Q \times \mu \times L]/ A \times (P_0 - P_1) \tag{7}$$

K_a = air permeability (m^2)

Q = flow rate (m^3/sec)

A = effective cross sectional area of sample

P_0 = inlet pressure (Pa)

P_1 = outlet pressure (Pa)

Springer (1993) determined the air permeability of porous material based on the following assumptions:

1. air permeability can be derived can modified version of Darcy's law
2. steady-state flow conditions exist
3. isothermal conditions exist in the soil
4. diffusive air flow within the soil is negligible
5. there are no macropores or continuous air gaps between the sample and the test cylinder (i.e wall effects are negligible)
6. gravitational effects contributing to air flow are negligible
7. slip flow is negligible

The air permeability equation derived by Springer (1993) was based on Darcy's equation under the above assumed conditions as shown below:

$$K_a = [Q \times 2 \times \mu \times L \times P_0]/A \times (P_0^2 - P_1^2) \tag{8}$$

$$K_a = A/B \tag{9}$$

where $A = Q$ and $B = [2 \times \mu \times L \times P_0/A \times (P_0^2 - P_1^2)]^{-1}$. The slope of the best-fit line to a plot of A versus B equals the air permeability for a given soil. The Springer equation considers the compressibility of the air while the Darcy equation assumes incompressible fluids. Hence, Springer equation is the fundamental equation for measurement of air permeability of the soil.

Table 2.3 shows the intrinsic permeability of different type of soil (Bear, 1972).

Table 2.3 Intrinsic permeability of different types of soil (Bear, 1972)

Permeability	Pervious			Semi-Pervious			
Sand & Gravel	Well Sorted Gravel		Well Sorted Sand or Sand & Gravel	Very Fine Sand, Silt,			
Clay				Peat		Layered Clay	
K (m^2)	10^{-7}	10^{-8}	10^{-9}	10^{-10}	10^{-11}	10^{-12} 10^{-13}	10^{-14}

CHAPTER 3

LIGHTWEIGHT CELLULAR CEMENTED CLAY

3.1 LITERATURE REVIEW

Horpibulsuk et al. (2003) showed that the strength equation for lightweight cellular cemented clays at particular water content was proposed based on Abrams' law (1918) as follows

$$q_u = A/(V/C)^B \tag{10}$$

where q_u is the unconfined compressive strength, V/C is the void/cement ratio, and A and B are constants. The A-value is dependent mostly upon the curing time. As the water content increases, the A-value decreases. The B-value is practically constant and equal to 1.20 to 1.29. The above equation is applicable for cement stabilised clays as well as lightweight cellular cemented clays which show that the parameter V/C can be used to analyse the strength and compressibility of lightweight cellular cemented clays. The parameters A and B should be pre-determined for its application for finding the strength of lightweight cellular cemented clay. The parameters A and B can be back calculated from at least two trial sample strength data. Thus, target strength can be achieved by varying the V/C ratio accordingly for given water content.

Oh et al. (2013) showed that air bubbles are first foamed by a bubble generator and then mixed with cement slurry. This pre-foaming method can easily control a number of air bubbles. A bubble generator was made and used for this test. This device is composed of a high-pressure pump, air compressor, mixer tube, and foam tube. The high-pressure pump is used to pump out diluted foaming agent. The air bubbles were foamed at an air compressor pressure of 400 ~ 450 kPa. The diluted foaming agent and air are mixed in the mixer tube. During this process, the air compressor supplies pressure to make bubbles in the foam tube. Similar, procedure can be adopted in the formation of controlled air bubble in the cement-clay slurry. He showed that the effect of vibration on the early stage of light weight air entrained soil. He showed that vibration velocities of 0.25 and 0.50 cm/s did not greatly affect the strength in the early stages of curing. However, vibration velocities of above 2.50 cm/s significantly affected the decrease in strength.Many construction sites have seen a rapid increase in the number of vibration-related problems. There are various types of vibration: instant shocks due to explosions; blasting in

mines or construction sites according to the source; excavation, machine tools, and motors; constant shocks due to pile driving and vibrations caused by transport facilities such as vehicles and machines. Such vibrations affect the safety of existing structures. He concluded that the specimens that did not experience vibration had a sleek and homogenous surface, whereas specimens exposed to medium-magnitude vibrations or lesscured specimens that were vibrated had a white wavy pattern on the surface as shown in Fig. 2.4. Specimens exposed to high-magnitude vibrations or specimens that were vibrated in the slurry state had large cracks. In addition, the height of the specimen decreased with material segregation of the sand and air bubbles because the air bubbles in the bottom layer of the specimen in the mold could not escape, while air bubbles in the upper–middle layers were emitted when vibrated.

| (a) vibration free | (b) medium- magnitude of Vibration at fresh state | (c) large- magnitude of vibration at little cured state |
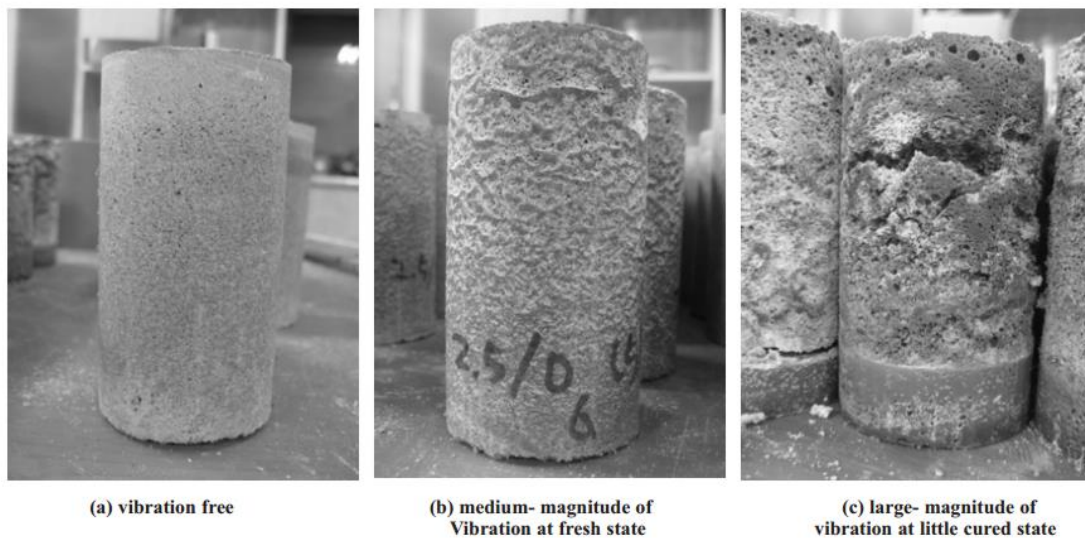
Fig. 3.1 State of LWCCC specimen according to vibration velocity (Oh et al., 2013)

Satoh et al. (2001) have developed lightweight treated soils for reuse of dredged soil as artificial lightweight geomaterials in coastal construction projects, the density of which range from 1.0 ~ 1.2 g/cm^3. In this case, light weight treated soil was directly placed underwater using a pusher pump and a tremie pipe. In the case of large tidal changes, the lightweight soil should be placed at larger depth underwater. The 1-year strength of light weight treated soil increased 40% over the 28-day strength. The wet density of lightweight soil measured 1 year after the construction showed a nearly constant value compared to the specimen of 28 days. One of the applications of light weight treated soil that was performed was in Kumamoto port located on the Ariake Sea on

the Kyushu Island of Japan. An extremely soft clay layer of 40 m thickness was deposited at the seabed. The construction of Kumamoto Port has a major engineering problem of low bearing capacity and large compression of the thick clay layer. In Kumamoto Port of Japan, new quay wall to the depth of 10 m below the sea level was proposed in 1979. The cost of the soil improvement has been accounted for more than 50% of the total construction cost. It was concluded that the usage of lightweight soil for the backfill would reduce the construction cost by 25% compared to the conventional method. The underwater placing of lightweight treated soils was performed inside the cells of the concrete caisson. He concluded that wet density of lightweight treated soil is an important index to control the quality in placing tests. It is observed that air foam disappears when it reacts with the organic matter in the soil. Hence, lose of air foam during mixing, transportation and underwater placing must be compensated for by adding extra volume in advance.

Kikuchi et al. (2011) have presented that water bleeding channels will tend to form if the air content is excessively large, so the wet density and coefficient of permeability will tend to increase. On the other hand, when the air content is small, the lightweight cellular cemented soil functions as an impermeable medium.

Indraratna et al. (2014) have studied recycled concrete as a material which can be used as PRBs for the treatment of acidic ground water. Recycled concrete can be a suitable material for reactive media as it has the ability to remove Al and Fe effectively out of solution and thus maintaining the neutral pH. The performance of PRBs has been reduced because of reduction in pore space as mineral precipitation (mineral fouling) in reactive media.

Miki et al. (2003) presented that lightweight foam mixed in-situ surface soil as an embankment on soft ground was constructed with a target density of 0.8 g/cm^3 and unconfined compressive strength of 600 kN/m^2. Foamed mixed soil has been used extensively in Japan for road widening and back-filling projects. Greater surface area of cement/clay mixes has a greater water demand than cement/sand mixes. Usually, the total cement content lies between 300 to 500 kg/m^3.

3.2 PERMEABLE REACTIVE BARRIER

Groundwater (GW) is a natural resource of inestimable value. It contributes to the maintenance of the aquatic and terrestrial natural environments. Contaminated GW degrades the environmental quality and poses a risk to public health. Remediation of this contaminated GW has proven to be an important and challenging problem. Though the immediate need was compensated by 'Pump-and-Treat' technique, limitations such as high energy requirements, the risk of contaminant exposure still exist, and that is why there is a need for an innovative solution in this area. Permeable reactive barriers (PRB) are one of the most innovative, promising and green engineering approach. This concept is first developed by the University of Waterloo in the early 1900s. As per U.S. EPA(2001), a PRB is defined as, "*an emplacement to reactive materials in the subsurface designed to intercept a contaminant plume, provide a path flow through it, and transform the contaminant(s) into environmentally acceptable forms to attain remediation concentration goals down gradient of the barrier*".
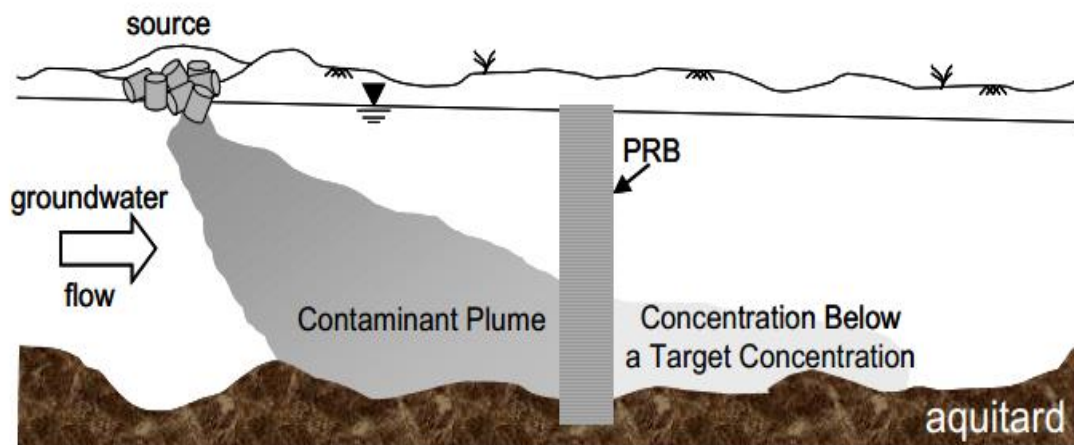
Fig.3.2 Schematic view of a typical permeable reactive barrier PRB (adapted from Tratnyk et al., 1997)

The most common approach of installing a PRB in the field is to excavate and fill a trench with appropriate reactive materials. In general, PRBs are aligned perpendicular to GW flow, as shown in Fig. 3.2. As the contaminants flow towards the structure by ambient GW flow, the materials there enhance the physio-chemical reactions that remove the contaminants. The physico-chemical reactions include adsorption, ion-exchange, precipitation, or oxidation-reduction (redox) reactions. In some cases, the materials act as a source of energy for

microorganisms, which breakdown the contaminants to a less toxic form. PRBs are considered as a contaminant technology because they restrict the transport of contaminants. However, PRBs do not impede the flow of GW because the hydraulic conductivity of the PRB is greater than the hydraulic conductivity of the aquifer.

PRBs have been proposed for containment of many contaminants including the heavy metals, radioactive waste, petroleum products, industrial chemicals (Cantrell et al., 1994; Blowes et al., 1995). Each contaminant may require a unique media, but the principle of transforming or immobilizing contaminants as they pass through the PRB is the same regardless of the target contaminant. PRBs are designed to operate passively for several decades. This is perhaps the biggest advantage of PRBs are long-term operation and maintenance costs are minimal and there is no chance of mechanical failures causing the system to shut down. In these methods, the contaminants are treated without soil excavation or water pumping. Generally, this cost-effective clean-up technology impairs the environment much less than other methods. A disadvantage of PRBs is that there is limited guidance for their design and monitoring.

The main configurations for systems with permeable reactive barriers are (Golder Associates Ltd. 1998):
• continuous reactive barriers,
• funnel-and-gate systems,
• arrays of wells filled with reactive materials,
• injected systems.

The two main configuration types of PRBs that have been used are the "funnel and gate" and the "continuous gate design". The funnel and gate, which consists of cut-off walls meant to converge the plume to the treatment zone, and the reactive gate in which the treatment occurs. Even though this configuration type is expensive to construct compared to the latter, it allows for pockets of plumes widely distributed to be captured for treatment. The continuous gate configuration, on the other hand, involves the placement of the treatment barrier across the entire contaminant plume path. The merits of this configuration type are that it is easy to construct, less expensive and has little effect on the groundwater flow.

The basic requirements the structure of a reactive barrierhas to fulfil arehigher permeability than the surrounding reservoir, replaceability of the reactive materials, stability against fines transported into barriers from the surrounding soil and long life-span.

Till now various contaminants have been used but less amount of research has been done in lightweight cellular cemented clay as a PRB.

3.2.1 *Existing technologies in Permeable reactive barrier*

There are large number of types of existing PRB reactive material that can be used. But, the zero-valent iron (ZVI) is the most frequently utilized media both in laboratory studies and field applications. ZVI has a high reduction potential. ZVI has been extensively used for the removal of chlorinatedsolvents such as TCE (trichloroethylene) and PCE (polychloroethylene). These contaminants mostly act asoxidants and thus are readily reduced by ZVI via transfer of electrons in anaerobic conditions. Others, including activated carbon(AC), zeolites, peat, sawdust, oxygen releasing compounds(ORC), etc. have also been used and evaluated. The limitations withmost of these materials, however, are that they are expensive, difficultto access or effective for only certain groups of contaminants. Biobarriers are a type of PRBs filled with materials that stimulate or enhance microorganisms to degrade contaminants aerobically or anaerobically.

Recycled concrete is seen as a promising material as PRB. Lightweight cellular cemented clay hence, becomes important as an alternative to recycled concrete in PRBs because it's more or less similar mineral (cement) composition. When the ground water/soil contains different types of contaminants, then removal of all contaminants is not possible by a single reactive barrier. Then, multiple reactive barriers will have to be used in which combination of different types of reactive material can be used.

3.3 APPLICATIONS OF LWCCC

Structural lightweight materials are an important and versatile material, which offers a wide range of technical, economic and environmental-enhancing and are designed to become a dominant material.

When infrastructures such as road embankments and bridge foundations are constructed on soft soil deposits, several geotechnical engineering problems are encountered. These deposits tend to

consolidate and undergo large vertical settlement and lateral deformation during and after construction due to incumbent loads. The problems are moreover related to short-term and long-term stability when an unexpected loading (e.g. earthquake) is imposed on the structures and soft ground system. To solve these problems, the improvement of the soft ground by the deep mixing technique of cement admixed clays is done. Instead of improving the soft ground (foundation), the use of lightweight materials with moderate to high strength as a backfill material to reduce the weight of the structure on the soft clay is an effective alternative means.In cooler climates, motorways and aircraft runways are usually air entrained to withstand freeze-thaw cycles and shrinkage cracking. Air entrained concrete allows the expansion during freezing of water in air voids to take place without causing any further stresses, as the air bubbles are capable of being compressed.

These lightweight materials have wide applications in the infrastructure rehabilitation and in the construction of new facilities. A lightweight cellular cemented soil (LWCCC) is a mixture of in-situ soil, cement and air bubbles. These can be used as a backfill for bridge abutments to reduce the earth pressure behind the wall, as a fill for construction on the soft soil to reduce the overburden pressure and as a method for reducing the pressure on tunnel lining. In addition to these, they also enhance the bearing capacity and reduce settlements.The first lightweight material was used in Oslo, Norway, where expanded polystyrene (EPS) was utilized in road embankments on soft ground. The advantage of LWCCC is cost-effective in terms of its construction time, material and transportation.

3.4 STEPS INVOLVED IN MANUFACURING OF LWCCC

The process of manufacturing of LWCCC includes mixing of soft clay with water to obtain clay slurry. This clay slurry is pumped into a mixing chamber and mixed with Portland cement. The cement-clay mixture is then transferred to an air foam mixing plant and mixed with air foam to have a high workability (high flow value) and low density. LWCCC can be transferred directly from batch plant to site by pumping due to its high fluidity. This material doesnot require compaction and saves the transportation cost of selecting suitable granular backfill material from distant sources. Also with time, its strength, stiffness and Poisson's ratio increase providing further more resistance to the lateral movement. The air bubble cannot enter into the pore space of the moist clay unless the water content is sufficiently high to reduce the attractive forces

between the clay particles. It is thus impossible to make an LWCCC at low water content. The optimum water content is about 1.9 times the liquid limit. The equation proposed by Horpibulsuk et al. (2012) based on Abrams' law was proved as a suitable for predicting the unit weight of the LWCCC with different water contents, cement contents and air contents.

Ceraplast AER

Ceraplast AER is air entraining admixture based on neutralized synthetic resin with compatible surface active agents to produce microscopic air bubbles, which makes the cemented soils easier to work and spread. Advantages of Ceraplast AER include improved workability, reduction in bleeding and segregation, pumping aid to maintain cohesiveness when concrete is pumped, converts harsh mixes into cohesive mixes and increases resistance to freeze-thaw effects. Ceraplast AER entrains numerous micro air pockets of less than 2 mm diameter (Cera-Chem Pvt. Ltd., Jan 2014).The supply form of Ceraplast AER is in a liquid state. Its colour is light brown. Its specific gravity is 1. Its chloride content is nil. It lowers the surface tension of water and makes cement particles hydrophilic, resulting in excellent dispersion as well as controls the setting of concrete, depending on dosage. This increases the workability of concrete drastically and also facilitates excellent retention of workability. The workability offered at a lower water-cement ratio eliminates chances of bleeding, increased workability; retention allows increased travel time at sites (Kanagalakshmi et al., 2015).

As the cement content increases and air content decreases, the unit weight and unconfined compressive strength of the clay increases. Higher voids (air and water) and lower amount of soil solids are associated with lower strength. In other words, the lower the water content means the strength has ahigher value.A key parameter for the lightweight cellular cemented clay at different weights of soil is thus proposed as water-void/cement, $w - V/C$. This parameter is defined as the product of initial clay water content (before mixing with cement and air foam) times V/C, where the water content is expressed in decimal.

On the basis of literature review conducted, following are the steps for manufacturing of LWCCC:

Mix design:

- Mix design of LWCCC should be prepared for the different amount of cement and air content. The sample can be prepared in cylinder tube having a diameter equal to have of it height so that unconfined compressive strength can be performed on it.

- The water content can be taken as 2 times the liquid limit of clay. But water content should be maintained same for all the different mix design. Only cement and air content should be varied. The cement content C, can be varied from 150 to 400 kg/m^3 of clay volume and the air content, A_c, from 10 to 100% of clay volume. The amount of liquid air entraining agent (Ceraplast AER) added along with the type and time of mixing will affect the air content. The volume of air entrained can be calculated as the difference between final mix volume of clay+cement+water+air bubbles and initial mix volume of clay+cement+water.

Steps involved in manufacturing of LWCCC:

- Cement and clay have to be mixed in abowl.

- Water should be added to it to make wet slurry at 2 times theliquid limit of clay.

- Air bubbles have to be generated by mixing Ceraplast AER and asmall amount of water in mixer/beaker.

- Mixing of air bubbles and soil slurry can be performed with the help of steel rod in a beaker.

- Calculate the wet density of cement+clay slurry and air content for different mix design. Wet density is calculated as the ratio of weight of wet slurry and volume of the wet slurry

- Shrinkage ratio should be found during the curing process for 1st seven days, 14th day, 21th day and 28th day of curing.

- Dry density should be calculated as the ratio of theweight of thedry sample and final volume of thesample after the LWCCC cures.

- Unconfined compression (UC) tests can be undertaken on samples after 7, 14, 28 days of curing.

- Variation of strength, unit weight and shrinkage should be plotted graphically for varying cement and air content.

Precautions to be taken while manufacturing LWCCC:

In case, at 2 times theliquid limit of clay slurry is not formed, then water content should be increased at say 3 or 4 times theliquid limit. But, the same water content should be added for all the different mix design of LWCCC.

- Mixing time will affect the amount of air bubbles generated in the mixture, hence mixing time should be same for all the different mix design.

- Mixing of air bubbles and soil slurry in mixer should be avoided as dissipation of air bubble might take place.

- Vibrating of the concrete can further reduce air content by 15 to 20 percent. Vibration of the sample should be avoided in early stage of curing (Oh et., 2013)

CHAPTER 4

DEVELOPMENT OF EXPERIMENTAL METHODOLOGY

4.1 DIGITAL IMAGE ANALYSIS

A unique method has been created to determine micro-structural properties of soil. The first step includes resin impregnation of the soil in order to make a specimen. This specimen was cut to create an observation surface for high quality image acquisition with the help of digital camera (make Canon EOS1200D, Japan). This high quality image is further processed using image processing techniques. Then analysis of the image is performed in order to get the micro-structural properties of soil such as porosity, particle size and pore size distribution. In the process, two different image processing software were used and results can be compared in order to conclude a better software. Fig. 4.1 shows the process followed in digital image analysis.

```
┌─────────────────────┐
│  Material selection │
└─────────────────────┘
          ↓
┌─────────────────────┐
│ Resin impregnation  │
└─────────────────────┘
          ↓
┌─────────────────────┐
│  Image acquisition  │
└─────────────────────┘
          ↓
┌─────────────────────┐
│  Image processing   │
└─────────────────────┘
          ↓
┌─────────────────────┐
│   Image analysis    │
└─────────────────────┘
          ↓
┌─────────────────────┐
│      Results        │
└─────────────────────┘
```
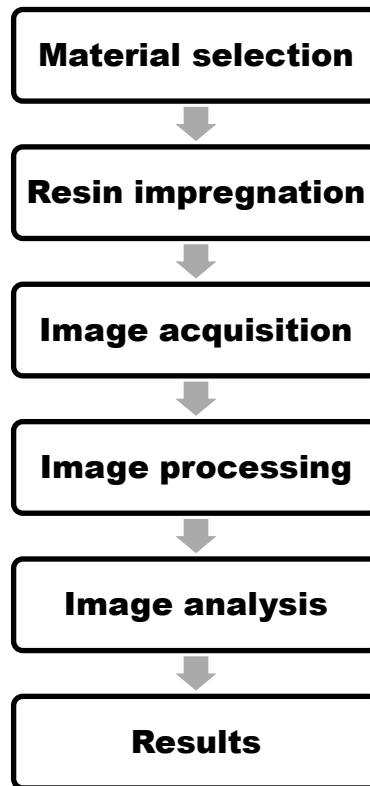
Fig. 4.1 Flowchart of process followed in digital image analysis

4.1.1 *Resin Impregnation Studies*

Epoxy resins are thermosetting polymer resins. Using liquid epoxy resins for preserving the integrity of the sample is a practical and relatively easy method as compared to conventional methods such as freezing. Jang et al. (1999) has studied about the use of epoxy resins for sand sample impregnation. Digital image analysis of resin impregnated samples has become an easy and reliable option. In present experiment, the liquid epoxy resin was used along with liquid hardener. The properties which are needed for the epoxy resin are low viscosity, room temperature curing and low shrinkage during curing, high bonding strength on curing and non-reactiveness with soil and test equipment. These requirements were met by the epoxy resin Araldite LY 556 and GY 257 which were used in the experiment.

The material chosen for resin impregnation was commercially available Indian Grade II sand (0.5-1 mm). Initially, resin impregnation was performed in sand samples but after cutting of these samples it was found out that the images that were acquired were not exhibiting good contrast between the resin (pore space) and particles. Hence, during the processing of image, difficulties are encountered giving rise to incorrect results. Hence, in order to improve the contrast, colour dying of resin was seen as a solution to this problem. In specimen without colour dye (Fig. 4.1a), the resin will act as a translucent medium by which when we see from top section we also see the particle that is below the top surface particle. This creates lot of difficulty in image processing. But in the sample with dye (Fig.4.1b and Fig. 4.1c), when we see from top section we will see only surface particles that are cut. Hence, colour dying of resin was preferred as compared to pure resin.
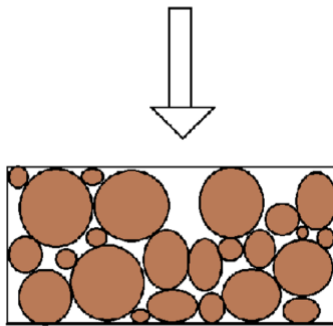
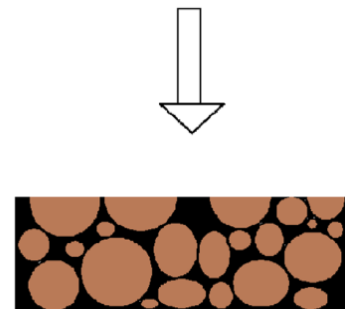**Fig. 4.1a Resin is translucent**   **Fig. 4.1b Before cutting specimen, resin is opaque; with dye**   **Fig. 4.1c After cutting the specimen**
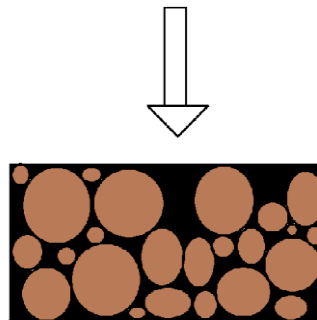
Various types of colour dyes were tested on the resin so that the best colour dye can be chosen. They were blue ink, food dyes, hair colour dye, $KMnO_4$ dye, Camlin paint, Ujala and Artline permanent black marker ink. The resin was dyed with the help of all the above colour dyes. Artline permanent black marker ink showed the best contrast between the resin and the sand particles. It was concluded that Artline permanent marker ink would give best results. Also, it was found out colour dying can be performed either by dying the sand or dying the resin. But dying of sand particles was not seen as aviable option since it would change the particle size and its surface properties. When cutting of sample is performed the sand gets cut it shows white colour and resin (pore) will show black colour. Thus, a good colours contrast is generated. The image processing of such images is much easier to perform so as to get better results.

The resin is present in the liquid state that is used as a medium to fill up the pore space of sand. It will become solid after a specific curing period when mixed with hardener. Initially, in the experiment conducted Araldite LY556 resin was used. The viscosity of this resin was high i.e. 10,000 mPa-s. Hence, the impregnation of epoxy resin through every connected pore in the sample required usage of the appropriate vacuum levels. Also, the surface of sliced samples was found to be uneven/ rough. The image of rough surface gives large number of blemishes and small spots. Hence, a new epoxy resin Araldite GY257 was bought which has a low viscosity of 500-650 mPa-s. The low viscosity resin has excellent surface penetration properties and it will ensure pore space is filled uniformly even in finer soils. The low viscosity resin has thus eliminated the use of vacuum during resin impregnation. The surface of specimen after cutting was found to be smooth. Table 4.1 shows viscosity of different types of resin and hardener and their mixture.

The hardener is also present in liquid state that is mixed with resin to make a solid specimen. The more the hardener content faster the solidification of resin takes place. Hardener used was HY951 having a viscosity of 10-20 mPa-s. The mixture of GY257 and HY951 has an ultra-low viscosity of less than 500 mPa-s. Hence, this mixture will fill up the pore space more uniformly than the mixture of LY556 and HY951. Ratio of resin and hardener is an important parameter that will affect the time period of solidification. Experiment at different ratios of resin to hardener by volume of 1:0.1, 1:0.2, 1:0.3, 1:0.5 and 1:1 were performed. The ratio was chosen such that curing time of resin is long enough to allow complete impregnation of resin in sand

sample and curing time of resin should be less time consuming. It is concluded that 1:0.2 would allow complete impregnation of resin in order to fill every pore of the sample and would solidify the resin within 12 hours of impregnation. Hence, ratio of 1:0.2 of resin and hardener is chosen as best mix ratio by volume.

Table 4.1 Viscosity of resin and hardener (Huntsman, 2012)

Materials			Dynamic viscosity @ 25°C (mPa-s)
Resin	Low viscosity	GY257	500-650
	High viscosity	LY556	10000
Hardener		HY951	10-20
Ratio of LY556 and HY951		1:0.1	1700
Ratio of GY257 and HY951		1:0.2	less than 500

4.1.2 *Specimen Preparation Procedure*

In order to prepare the specimen, the resin and hardener volume should be calculated. The volume of resin and hardener mixture is equal to the pore volume of the sand sample. The void volume V_v was calculated using equations 11, 12 and 13.

$$e = (G_s \gamma_w / \gamma_d) - 1 \tag{11}$$

$$\eta = (e/1 + e) \tag{12}$$

$$\eta = V_v / V_t \tag{13}$$

G_s = 2.65 for sand, V_v is the total volume of resin and hardener divided in 1:0.2 ratio, mass of resin and hardener is calculated from its specific gravity, specific gravity of HY951 = 0.98; Specific gravity of GY257 = 1.11 to 1.16. 10 percent of extra resin and hardener was added to account for any losses. Thus, we can calculate the amount of resin and hardener required for sample preparation.

Steps involved in preparation of resin impregnated soil specimen are as follows:

1. Covering of cylindrical steel tube with plastic sheet at the bottom of the tube.

2. Lubricating the inside portion of steel tube with oil/grease for ease of ejection of solid samples

3. Compaction of sand in 3 equal layers using steel rod in a steel tube.

4. Mixing of low viscosity resin and hardener in the ratio of 1:0.2 was done in a beaker.

5. Addition of 1 ml of Artline black permanent marker ink to the mixture

6. Pouring of resin-hardener mixture into the sand

7. Ejection of solid sample from steel tube after completion of curing for 12 hours

8. Cutting of horizontal sections of the solid samples

4.1.3 *Image Acquisition Techniques*

Image acquisition of the soil specimen has been performed by Digital Single Lens Reflex (DSLR) camera. The camera used was a CanonEOS1200D camera, equipped with Canon EFS (18-55 mm) lens for close range image acquisition as shown in Fig. 4.1d. The effective pixels size of optical sensor is 18 megapixels. The advantages of DSLR camera are high quality images, easy to use, affordable, reliable, and parallax-free as it is the single lens and better focus because of interchangeable lenses. Thus, it is easier to use when compared to highly expensive X-ray computed tomography and scanning electron microscope techniques. Fig. 4.1e shows image acquired using DSLR camera of the Grade II sand specimen with Artline black permanent marker ink as a colour dye.

Fig. 4.1d Canon DSLR camera 1200D along with tripod

Fig. 4.1e Image acquired using Canon DSLR camera, diameter = 39 mm

4.1.4 *Image Processing Techniques*

The image processing and image analysis were performed using the softwares Image J and Avizo fire. Image J is an open-source, Java-based freeware program widely used in geology, biology and astronomy and to perform particle analysis. Image J gives processing and analysis of a 2D image. Avizo fire can provide processing and analysis of both 2D and 3D images. In Image processing, the image is processed by using tools of software, so as to increase the contrast, remove small spots, create a binary image and separate the objects. After processing, analysis of image is performed so that results can be obtained. Fig. 4.1f to 4.1m shows the steps followed in Image J software. Fig. 4.1n to 4.1t shows the steps followed in Avizo fire software

Image analysis was performed in Image J by following steps:

1. The images obtained from a digital camera are colour (RGB) images which are converted to greyscale image using *Image-Type-8 bit*. Further, the scale of the image was adjusted by converting pixel into mm using a scale factor in *Analyse-Set scale*.
2. The brightness and contrast of the greyscale images are then auto-adjusted using *Image-Adjust Brightness/Contrast-Auto*, in order to ensure that all images are of equally good quality.
3. Finally, before converting to binary (BW) image thresholding is carried out by using *Image-Adjust-Threshold*.
4. Further, the images are filtered to remove noises and artefacts, and smoothen the particle perimeter by using *Process-Noise-Despeckle. Remove outliers* were to be performed multiple times to remove very small bright and dark spots interfering with particles.
5. Watershed segmentation of thresholded image is performed for separation of particles.
6. The analysis is performed using *Analyse-Measure*. Using this step the area of individual grains was calculated and the intermediate axis dimension of individual grains was determined.
7. Porosity, particle size distribution and pore size distribution were obtained using the analysis.

Image analysis was performed in Avizo fire by following steps:

1. Opening of image file
2. Volume rendering of the image is performed by *Volume rendering*

3. A square volume is extracted using *Extract Sub volume* so that the selected sub-volume can be analyzed

4. Ortho slice is performed using *Ortho slice* to define the axis aligned slice along the X, Y or Z axis of the image

5. The thresholding was performed automatically using *Interactive thresholding.* Ortho slice was attached to the thresholded image.

6. Image processing is performed to enhance the contrast and to remove spots and holes of the selected image. The following are the image processing tools used:

   a. *Remove small holes*

   b. *Remove small spots*

   c. *Smoothing and denoising ---->Despeckle*

7. Image segmentation that means separation of particles using *Separate objects* tool. Marker extent should be kept as 1 for better results.

8. Image analysis was performed using *Measure and analyse.*

   a. *Global measures----> Total pore area* in order to obtain the porosity

   b. *Individual measures----> Label Analysis---->Equivalent diameter, Area*

Fig. 4.1f Conversion of RGB colour image into 8-bit image, diameter = 39 mm
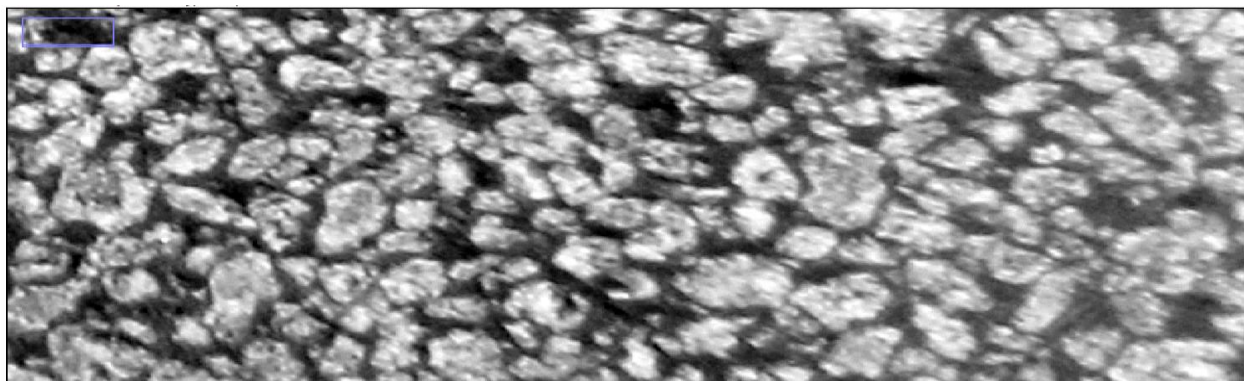
Fig. 4.1g Cropping of the image(15.7 mm× 4.8 mm)
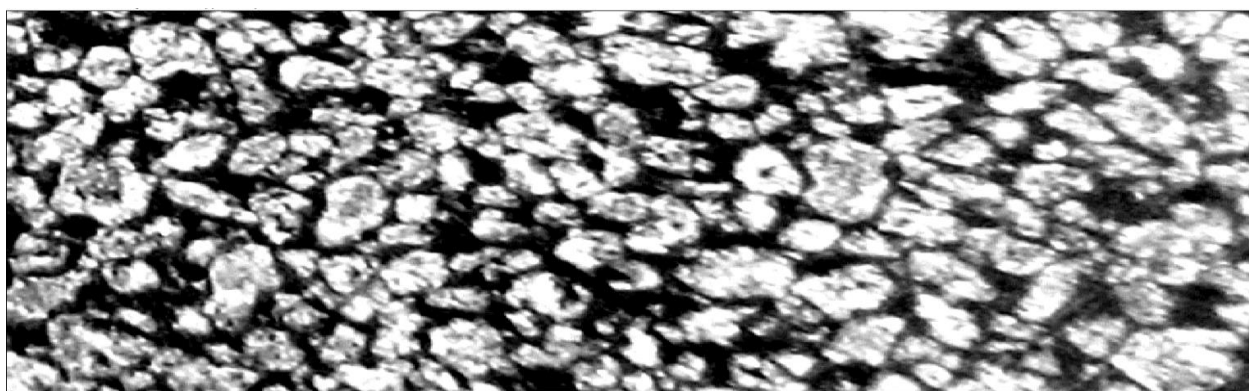
Fig. 4.1h Image enhancement(15.7 mm× 4.8 mm)
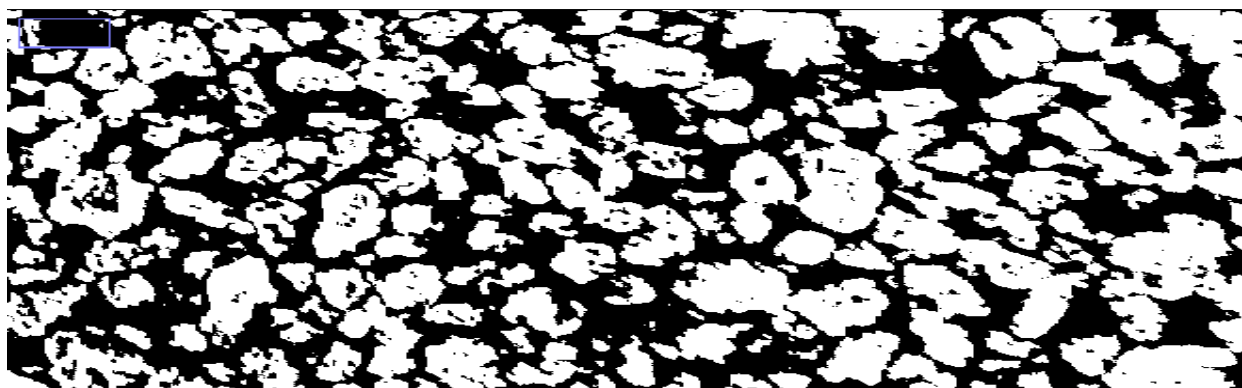
Fig. 4.1i Thresholded image using Shanbag method (15.7 mm× 4.8 mm)
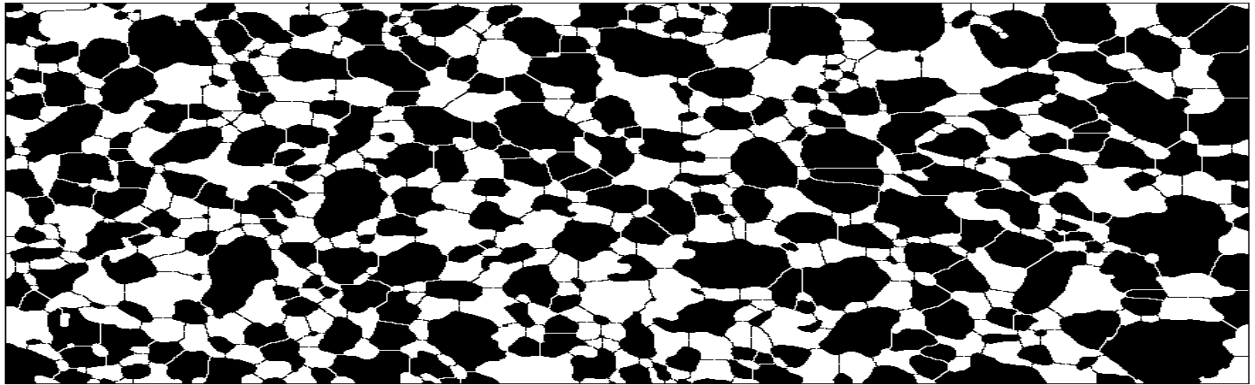
Fig. 4.1j Morphological operations and watershed segmentation(15.7 mm× 4.8 mm)
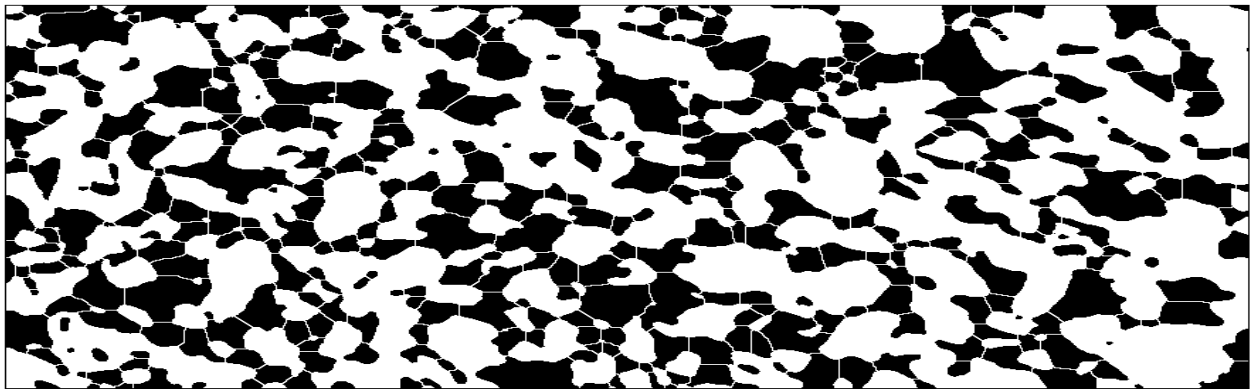
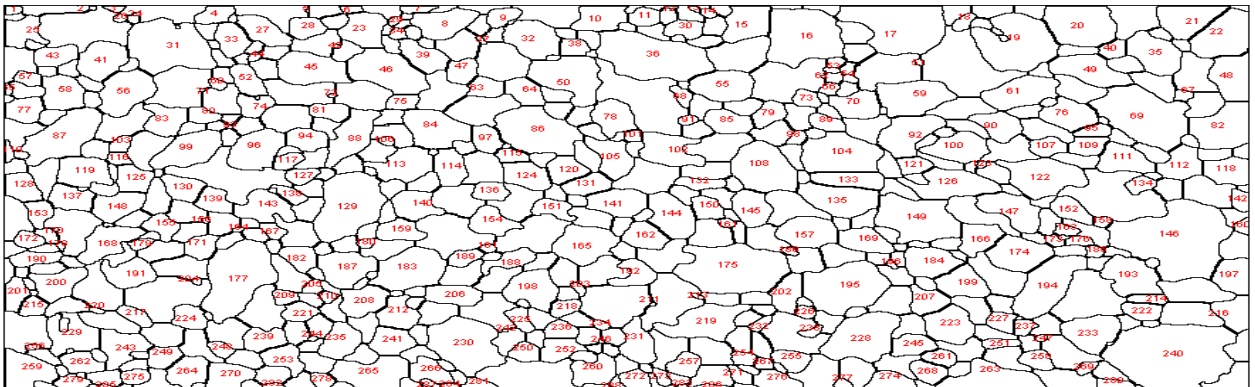**Fig. 4.1k Watershed segmentation for pores(15.7 mm× 4.8 mm)**
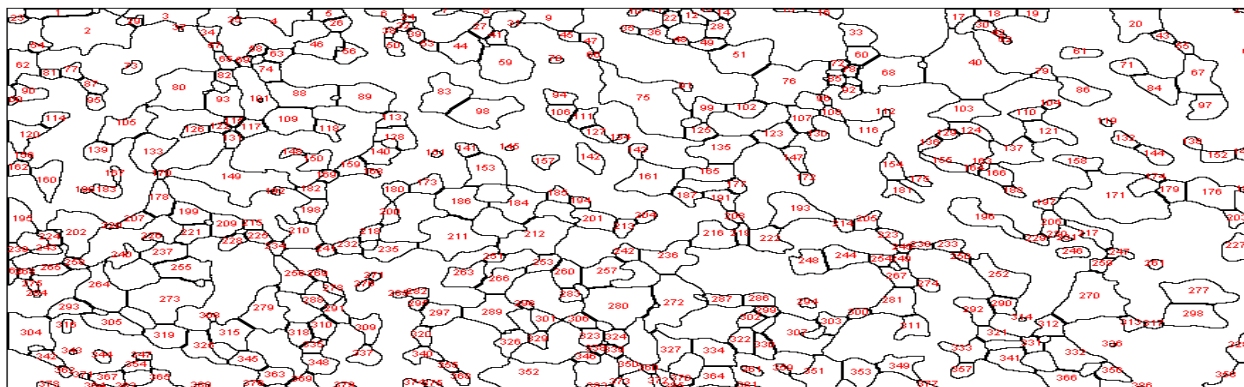

Fig. 4.1l Outlines for particles in Image J(15.7 mm× 4.8 mm)
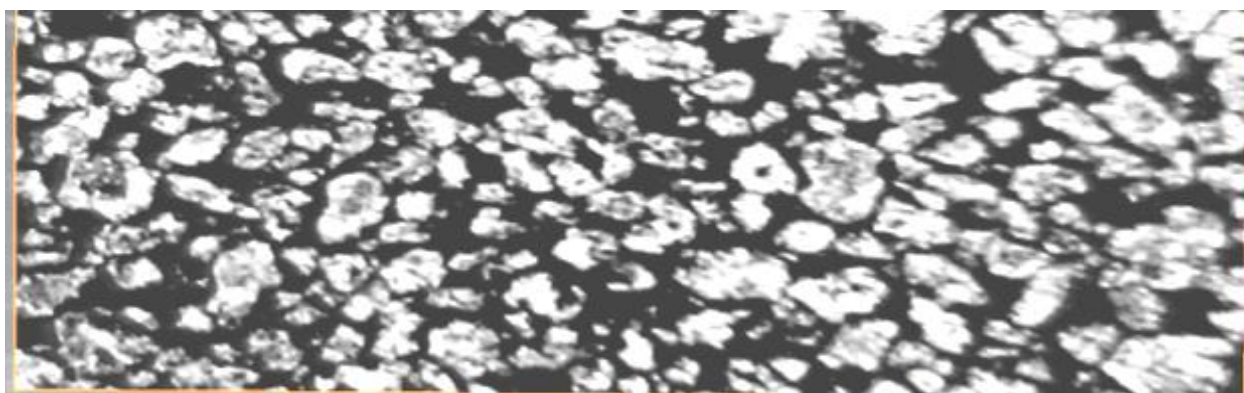
Fig. 4.1m Outlines for pores in Image J(15.7 mm× 4.8 mm)

Fig. 4.1n Volume rendered image in Avizo(15.7 mm× 4.8 mm)
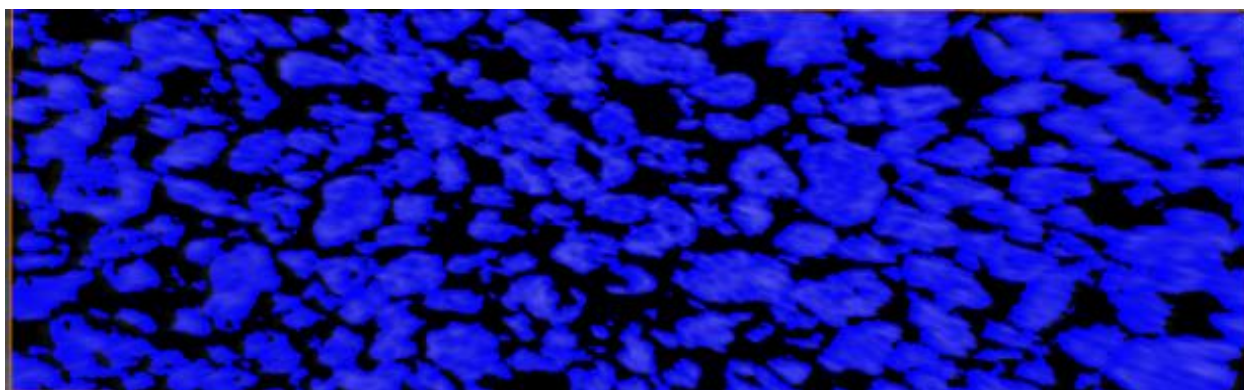
Fig. 4.1o Interactive thresholding of particles in Avizo(15.7 mm× 4.8 mm)
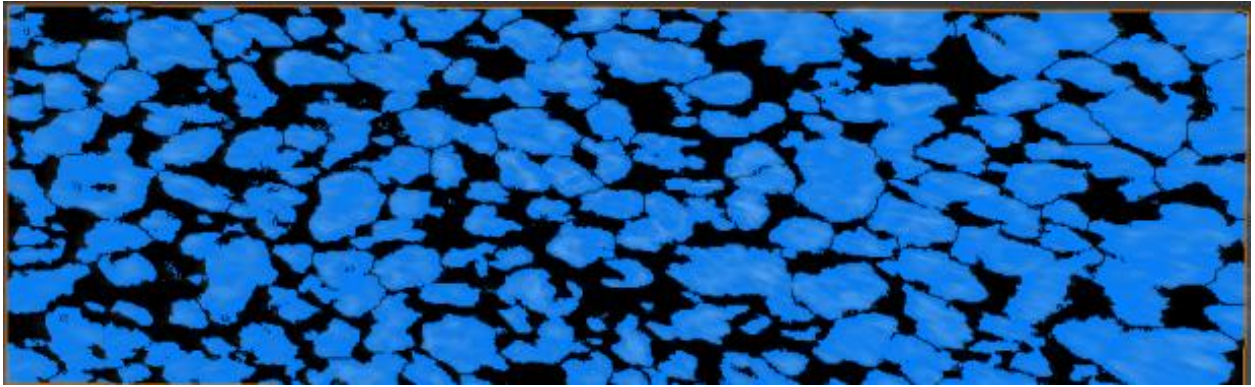
Fig. 4.1p Image segmentation(watershed) of particles in Avizo(15.7 mm× 4.8 mm)
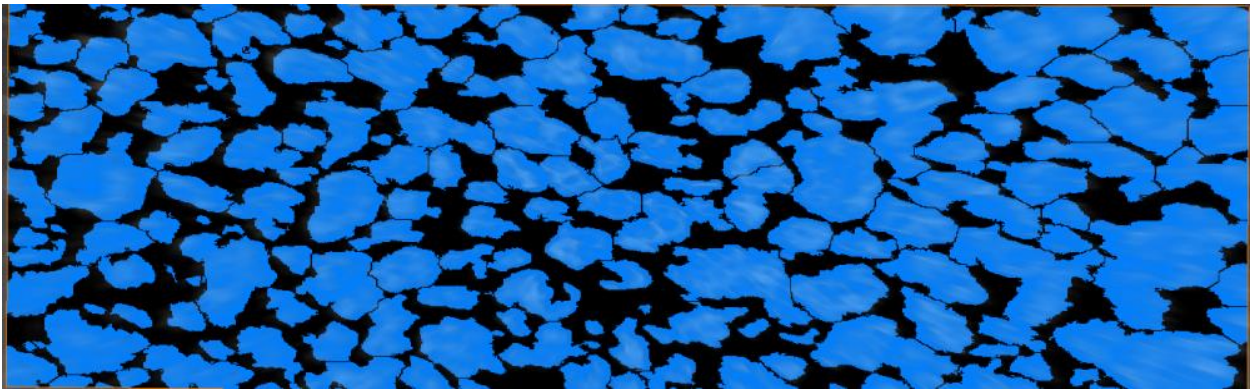
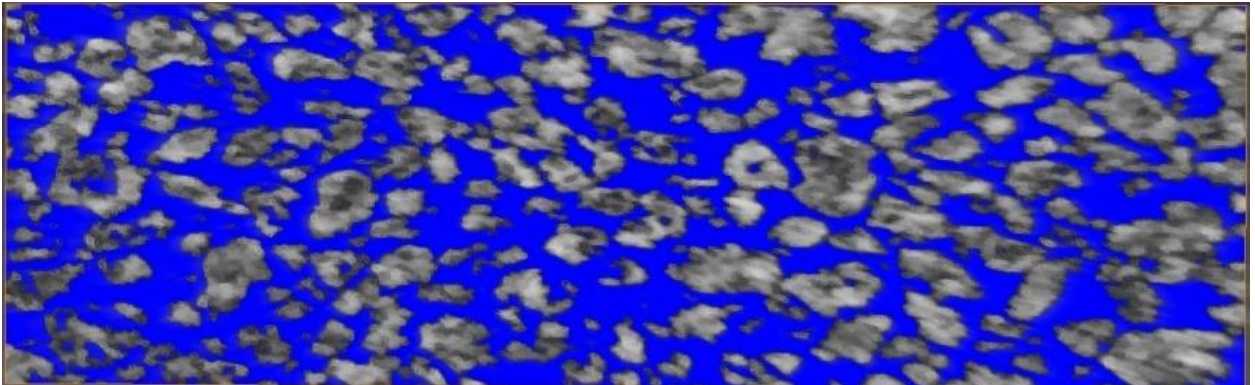**Fig. 4.1q Morphological operation of particles in Avizo(15.7 mm× 4.8 mm)**

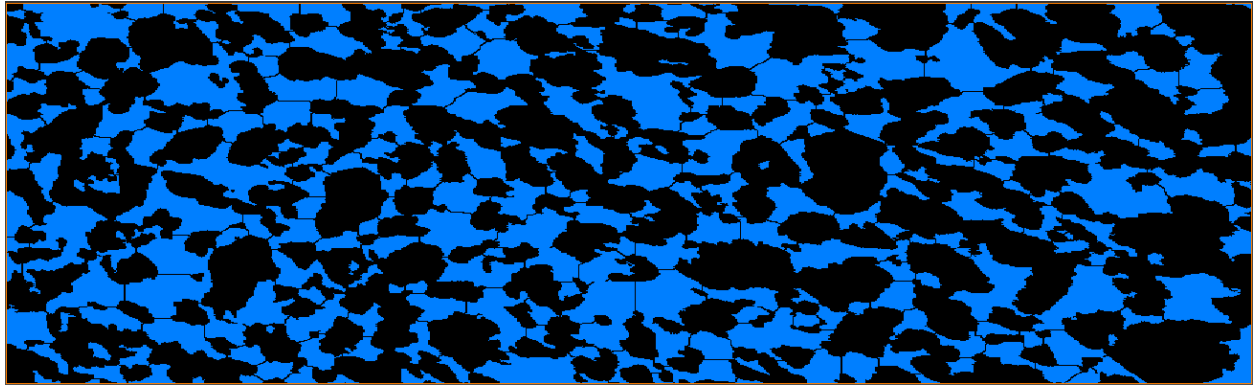**Fig. 4.1r Interactive thresholding of pores image in Avizo(15.7 mm× 4.8 mm)**

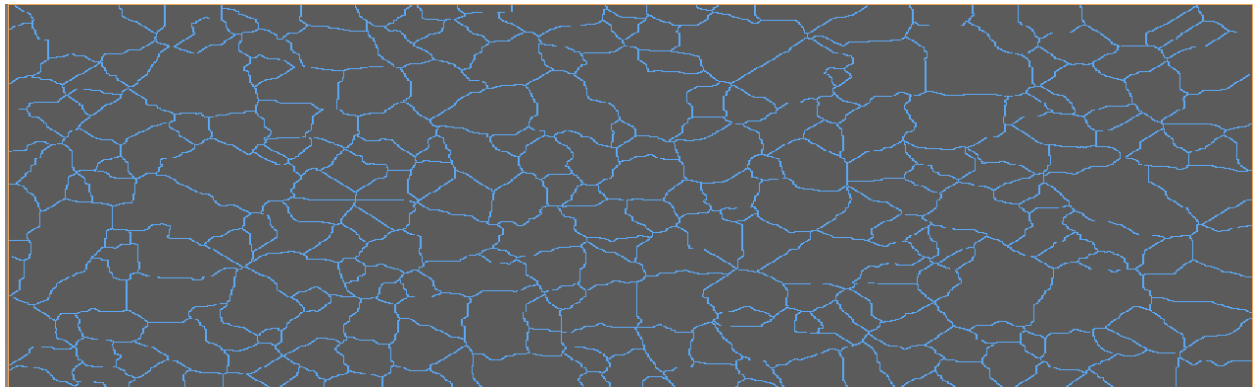**Fig. 4.1s Watershed segmentation of pores in Avizo (15.7 mm× 4.8 mm)**

Fig. 4.1t Pore lines generated in Avizo(15.7 mm× 4.8 mm)

In Avizo, it was observed that the particle area is included in the pore area. Hence, pore area is showing higher value than actual pore area as shown by pore lines. Hence, avizo is not able to give correct pore size distribution results.

4.2 DESIGN OF APPARATUS

The apparatus is designed such that air permeability, hydraulic conductivity and resin impregnation can be carried out on the same apparatus simultaneously. Air permeability and hydraulic conductivity of glass beads were found using the process shown in Fig. 4.2a. Five setups were designed and fabricated for different sizes of glass beads. For this experimental setup has been designed and fabricated, as shown in Figs. 4.2i, 4.2j and 4.2k and was referred from Richard long et al. (1998).
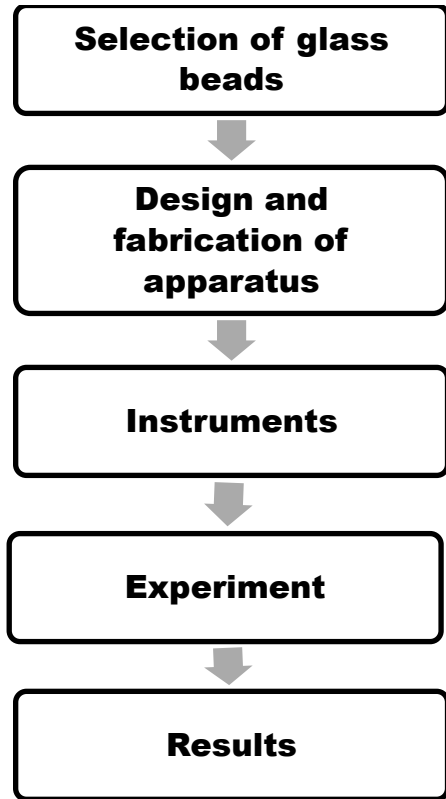
Fig. 4.2a Flowchart of process followed in air permeability and hydraulic conductivity experiment

The setup consists of steel tube of 47 mm inner diameter, 140 mm height, rectangular end plates, porous plate made up of acrylic on either side of the specimen, pneumatic push L-connectors at top and bottom end plate to allow fluid in and out of the specimen, connecting tie rods and O-ring arrangement to avoid the leakage. In the experiment, glass beads were used as test material. The glass beads were used as an experimental medium to serve as "control" sample where micro-scale processes which are affected by a variable soil texture, shape and size of pores, grain shape and packing can be minimized. All the glass beads of each size are a single-sized particle and hence in each setup single sized glass beads were present homogeneously. The five different sizes of glass beads are 0.46 mm, 1.29 mm, 2.36 mm, 3.075 mm and 3.6 mm as shown in Fig. 4.2b. Components used in the apparatus are shown in Fig. 4.2c to Fig. 4.2h.

0.46 mm   **1.29 mm**   **2.36 mm**

3.075 mm   **3.6 mm**

Fig. 4.2b Glass beads of different sizes

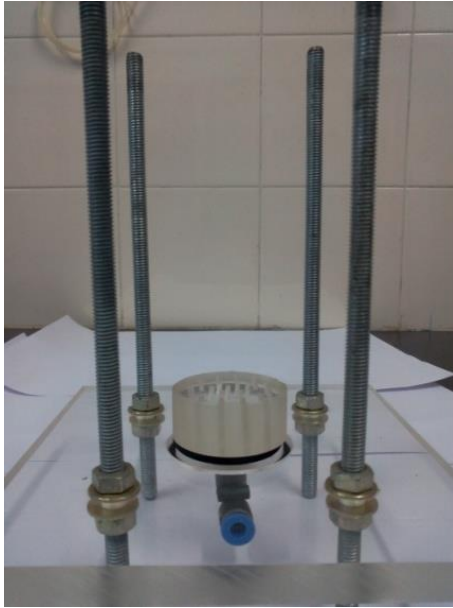**Fig. 4.2c Acrylic plate**

Fig. 4.2d Acrylic porous disc

Fig. 4.2e Steel cylindrical tube

Fig. 4.2f O-ring

Fig. 4.2g Fixing of L-connector flows valve, steel rods
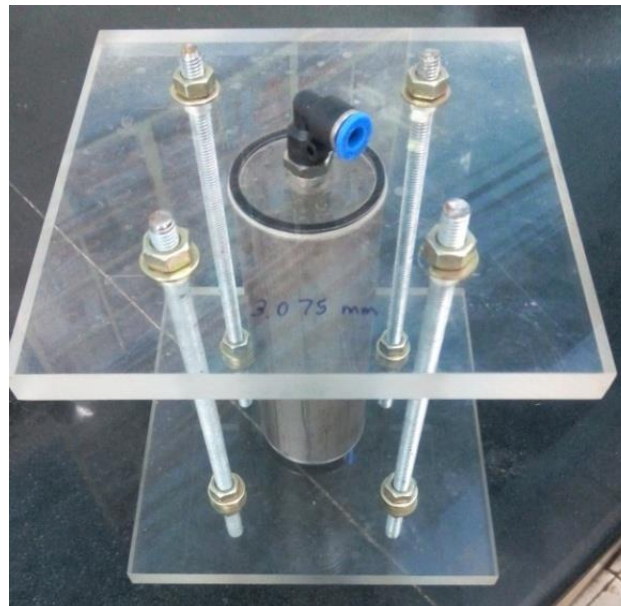
Fig. 4.2h Fixing of steel tube on O-ring

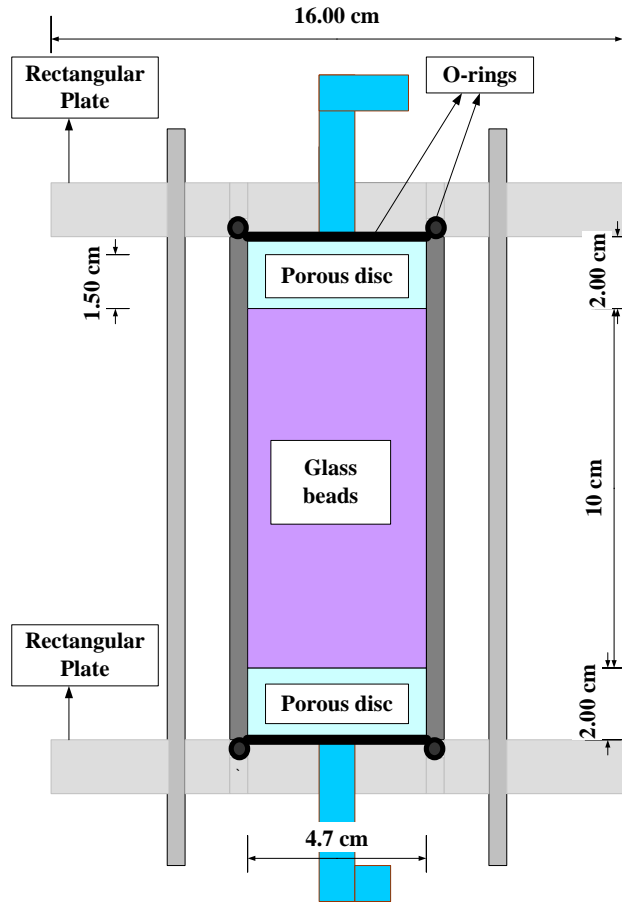**Fig. 4.2i Isometric view of permeability apparatus**

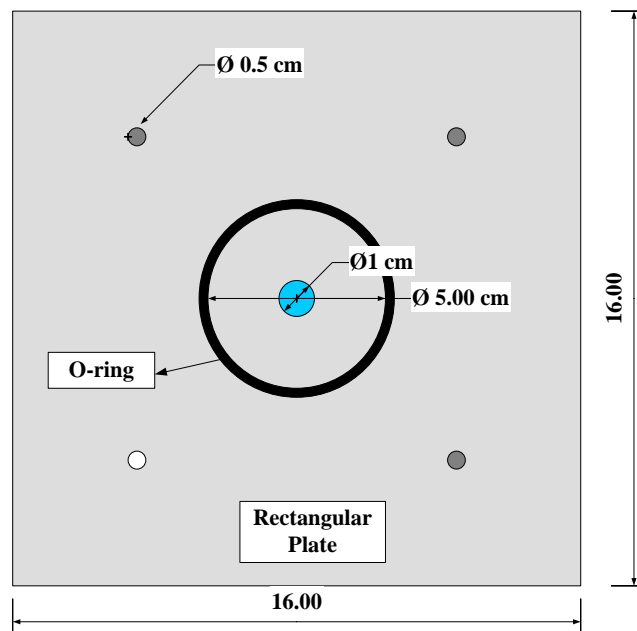**Fig. 4.2j Sectional view of permeability apparatus**

Fig. 4.2k Top view of permeability apparatus

46

In order to make the apparatus air and water tight, O-ring was attached at the bottom and top of steel tube. Filter cloth was placed above the porous disc in case of small particles of 1.29 mm and 0.46 mm so that particles do not pass through the porous disc vertical holes. The glass bead was poured in the apparatus using rainfall method. The apparatus was further used for hydraulic conductivity and air permeability experiment.

4.3 HYDRAULIC CONDUCTIVITY EXPERIMENT

The experiment is a part of establishing the relationship between air permeability and the hydraulic conducitivity of porous media. The experiment was performed on different sizes of glass beads. The falling head method experiment was performed on this apparatus to calculate hydraulic conductivity and was referred from ASTM International D 5084 – 10 (2010). The falling head method has an advantage over constant head method as it can be used for both fine-grained and coarse-grained soils.

Experimental procedure

The materials are fixed as shown in the Fig. 4.2j. The flow of water is kept from bottom to top of the apparatus. The pneumatic tubes were attached between the pneumatic L-connector valves and the falling head instrument. Any signs of leakage of water through tube or apparatus should be checked if present. Also air bubbles present in the tubes and apparatus have to be removed by allowing the flow of water through it for some time. The water is then allowed to flow through it and time between two heads of standpipe is measured using as stopwatch. A total of nine readings were taken for each head difference. The following formula was used for calculating hydraulic conductivity:

$$k = [2.3 \times a \times L \times \log(h_2/h_1)]/[A \times t] \tag{14}$$

where k = hydraulic conductivity in cm/s

L = length of soil specimen cm

a = area of standpipe in cm^2

A = cross sectional area of sample, cm^2

h_2 = initial head in cm

h_1 = final head in cm

4.4 AIR PERMEABILITY EXPERIMENT

The air permeability experiment was performed on the glass beads using the same apparatus as used in hydraulic conductivity. Green and Ampt (1911) found that intrinsic permeability (m^2) was the same when either air or water was used by using glass beads as media. The air permeability was based on the Darcy's law. The conventional method of finding air permeability included the use of U-tube manometer which had drawbacks such as low precision and time consuming. In order to increase the precision of reading, a combination of digital pressure sensor and data logger was used for measurement of pressure. This provided higher precision data collection in less amount of time. In addition, air flow meter was used for measurement of air flow rate. Thus, automation of air permeability experiment was performed.

4.4.1 *Physical Properties of glass beads*

The physical properties of the glass beads were calculated. The five different sizes of glass beads are 0.46 mm, 1.29 mm, 2.36 mm, 3.075 mm and 3.6 mm. Table 4.4b shows the Indian standard of classification of soils (IS 1498-2007). On the basis of this standard, permeable material (glass beads) were classified according to size. According to IS 1498-2007, 0.46 mm and 1.29 mm glass beads represent medium sand; 2.36 mm, 3.075 mm and 3.6 mm glass beads represent coarse sand. The specific gravity of solids (G_s) was calculated using helium gas pycnometer (shown in Fig. 4.4a as per ASTM D 5550-14 (2014) and the obtained results are presented in Table 4.4.

Fig. 4.4a Helium gas pycnometer present in BSB 125, IIT Madras

$$e = [(G_s \times \gamma_w)/\gamma_d - 1] \tag{15}$$

$$\eta = e / (1 + e) \tag{16}$$

The theoretical porosity was calculated using Eq. 15 and 16 and the results are presented in Table 4.4. In the experiment, the porosity of glass beads of different sizes is observed to be more or less constant from 0.38 to 0.39. It is because of the similar packing, shape and arrangement of glass beads.

Table 4.4a Particle size properties of glass beads using helium gas pycnometer

Diameter of glass bead	Specific gravity	Unit weight	Void Ratio	Porosity
3.6 mm	2.50	1.52	0.61	0.38
3.075 mm	2.51	1.52	0.62	0.38
2.36 mm	2.49	1.52	0.61	0.38
1.29 mm	2.51	1.53	0.61	0.38
0.46 mm	2.61	1.57	0.64	0.39

Table 4.4b Indian Standard of Classification of Soils (IS 1498-2007)

Coarse soils	Gravel size (G)	Coarse	20 - 80 mm
		Fine	4.75 - 20 mm
	Sand size (S)	Coarse	2 - 4.75 mm
		Medium	0.425 - 2 mm
		Fine	0.075 - 0.425 mm
Fine soils	Silt-size (M)		0.002 - 0.075 mm
	Clay size (C)		< 0.002 mm

4.4.2 *Experimental Setup*

The experimental setup includes pneumatic tubes, pressure cylinder, pressure regulator, and digital pressure sensor with a data logger, laptop, rotameter and permeability apparatus. Eureka made variable area flow meters (Eureka Industrial Equipments Pvt. Ltd, Pune, India) were used

in the experiment to measure the air flow rate in liters per hour which work on the principle of variable area as shown in Fig. 4.4c. It is equipped with a float that moves freely up and down in the tapered borosilicate glass tube with fluid flow from bottom to top. The float takes up a position where buoyancy forces and the float weight are balanced in proportion to flow rate. The vertical position of the float as indicated by scale is the measure of the instantaneous flow rate. In addition, pressure variation in the system was measured by Keller made pressure sensors with the help of National Instruments data logger with Lab view 2012. The pressure regulator is used for regulating the flow of air flow in the sample. Fig. 4.4e shows the block diagram that was created in National Instruments lab view 2012. Fig. 4.4f represents the flow chart of the entire experimental system with accessories. The experimental setup should be arranged properly as shown in Fig. 4.4c. Fig. 4.4g presents the online voltage amplitude versus time plot data logged by NI data logger for 1000 readings taken in 10 seconds.

Steps followed in the air permeability experiment are as follows:

1. Arrange the experimental setup as shown in Fig. 4.4f and the valve of rotameter is kept fully open to avoid generation of additional back pressure in the system.

2. Allow air to flow through the sample for 10 minutes so that air flow becomes uniform.

3. Adjust the air flow rate with the help of pressure regulator for 200 lph.

4. Measure the pressure with the help of pressure sensor and data log the values for 1000 readings

5. Convert the voltage to pressure using the calibration equation as shown in Eq. 15

6. Calculate the average air pressure P_1 from these 1000 readings taken.

7. A total of 3 trial readings of pressure for flow rate of 200 lph were taken

8. Similar, procedure should be followed for 300 lph and 500 lph air flow meter

9. Calculate the air permeability by substituting the value of air pressure P_1 in Darcy's equation as shown in Eq. 16

Fig. 4.4b National Instruments data logger

Fig. 4.4c View of Eureka air flow meter (66 to 680 lph)

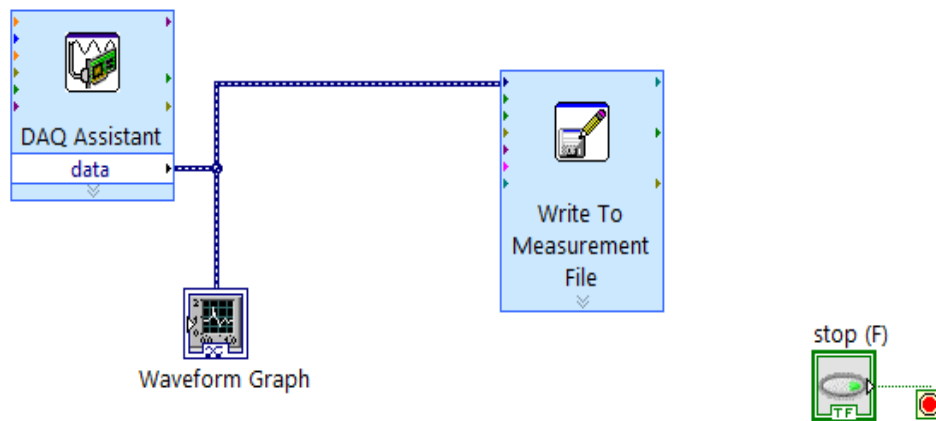**Fig. 4.4d Pressure regulator**

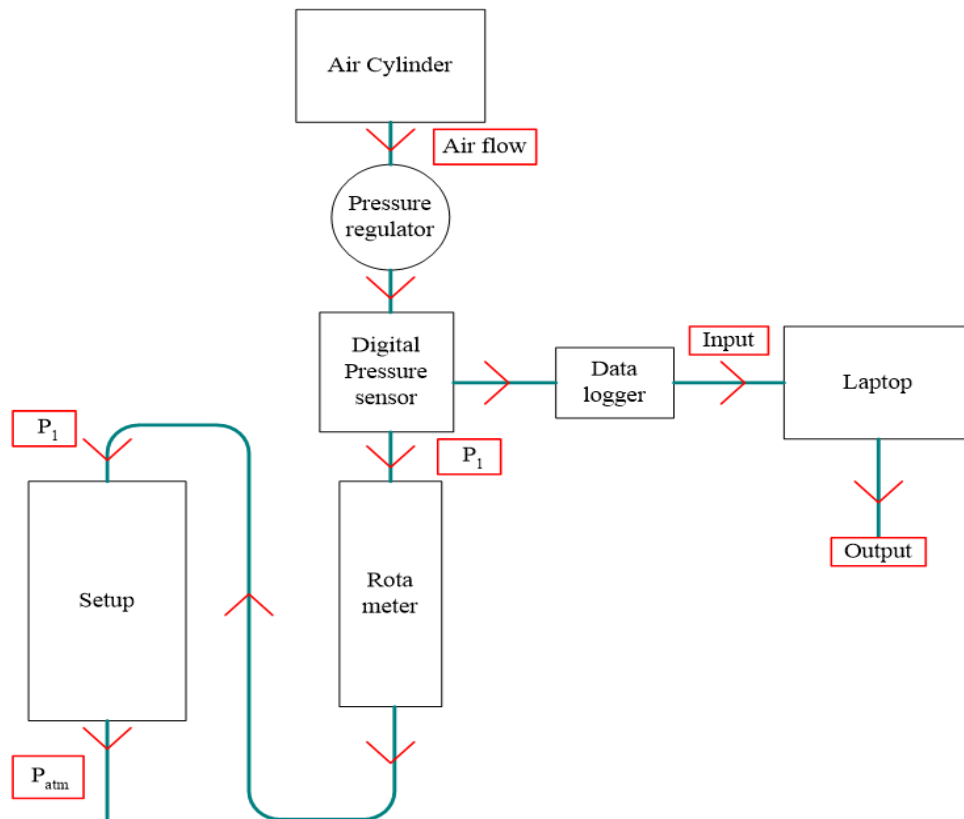**Fig. 4.4e Schematic view of the block diagram in National Instruments lab view 2012**

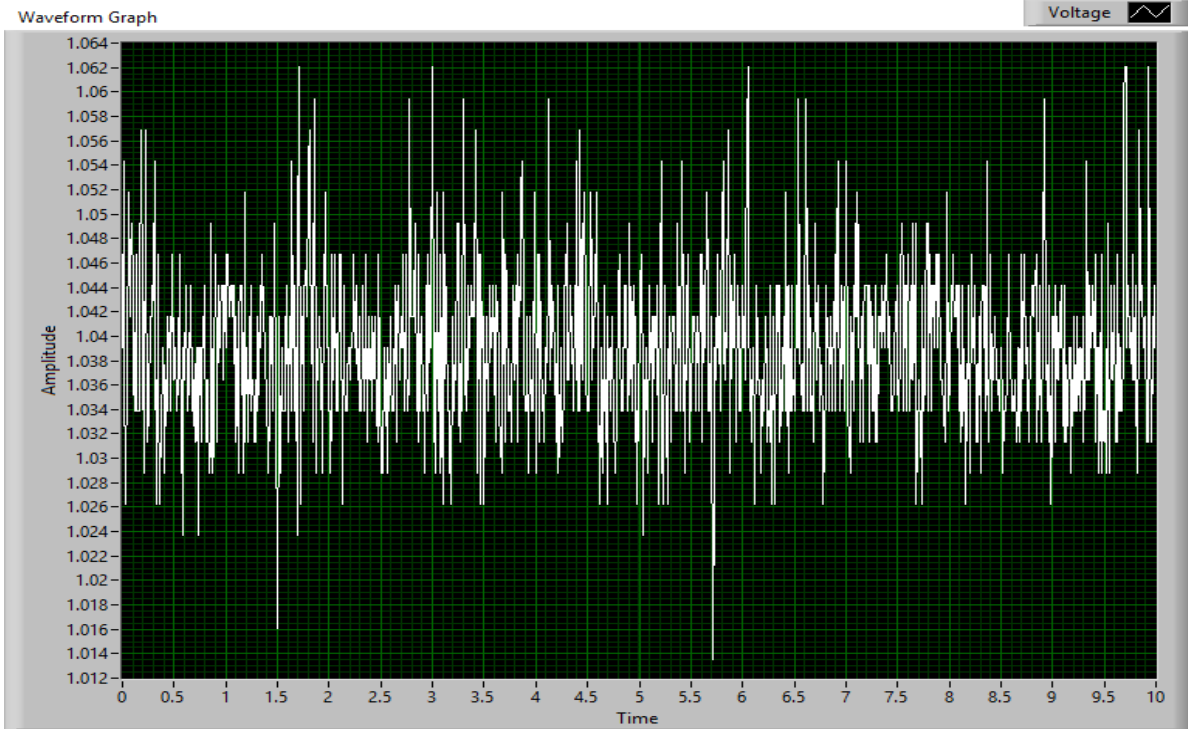**Fig. 4.4f Flow chart of experimental setup for Air Permeability**

Fig. 4.4g Voltage (Volts) Amplitude versus Time (sec), Lab view software

4.4.3 *Calculations*

The Keller made pressure sensor were calibrated with National Instruments data logger with Lab view 2012. The calibration is necessary so as to convert the obtained voltage values into pressure values. Eq. 17 shows the linear calibration equation where P is pressure in bar and V is voltage in volts. Calibration equation is as follows:

$$P\ (bar)\ =\ (1.5405)\ \times\ V\ (volts)\ -\ 1.5698 \tag{17}$$

Air permeability is calculated using Darcy's equation and the extended Darcy's equation provided by the Springer (1993) as shown in Eq. 18 and Eq. 19 below:

$$K_a\ =\ (Q\ \times\ \mu\ \times\ L)/\ \Delta p\ \times\ A \tag{18}$$

$$K_a\ =\ [Q\ \times\ 2\ \times\ \mu\ \times\ L\ \times\ P_0]/\ A\ \times\ (P_0^2\ -\ P_1^2) \tag{19}$$

The parameters used in Eq. 18 and 19 are shown as follows:

Length of glass bead specimen (L) = 8.8 cm

Diameter of specimen = 4.7 cm

Area of specimen $(A) = 17.35 \text{ cm}^2$

Dynamic viscosity of air $(\mu) = 1.79$ E-05 Pa.s

Air flow rate $(Q) = 200$ lph, 300 lph and 500 lph

RESULTS AND DISCUSSIONS

5.1 DIGITAL IMAGE ANALYSIS
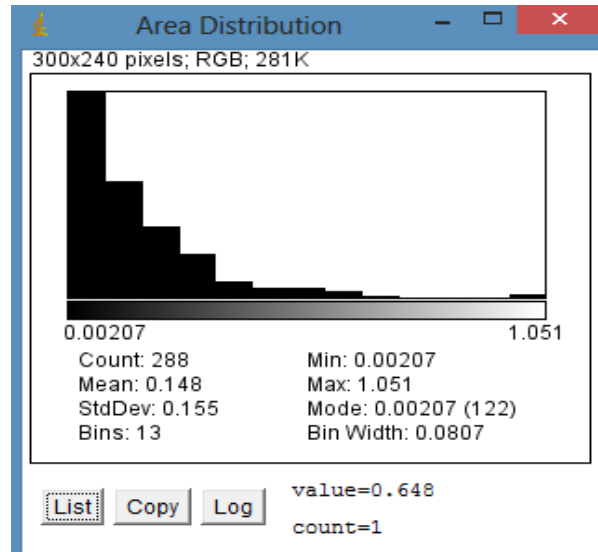
Fig. 5.1a Histogram of particle area of sand in Image J

Fig. 5.1b Porosity of sand is 40.59% in Image J
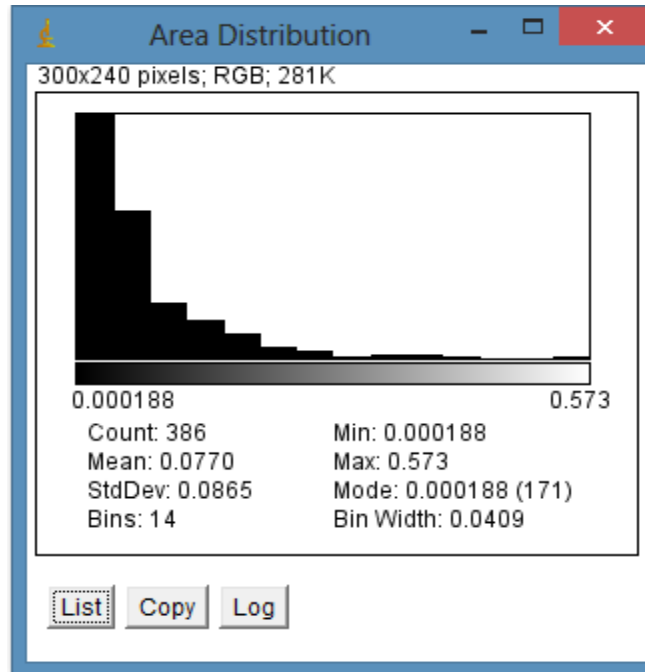
Fig. 5.1c Histogram of pore area of sand in Image J

Eq. diameter of particle (mm)
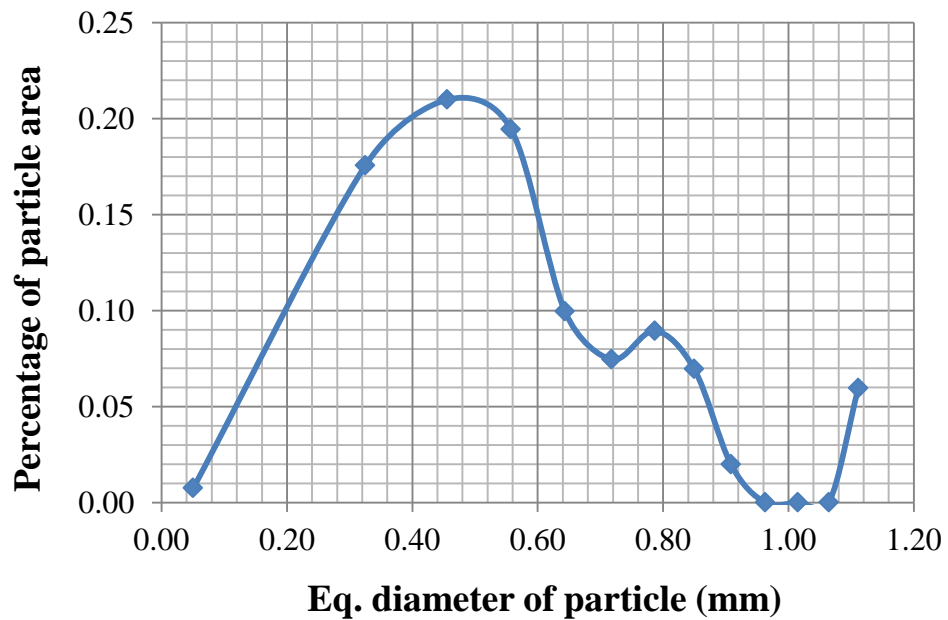
Fig. 5.1d Particle size distribution of sand in Image J
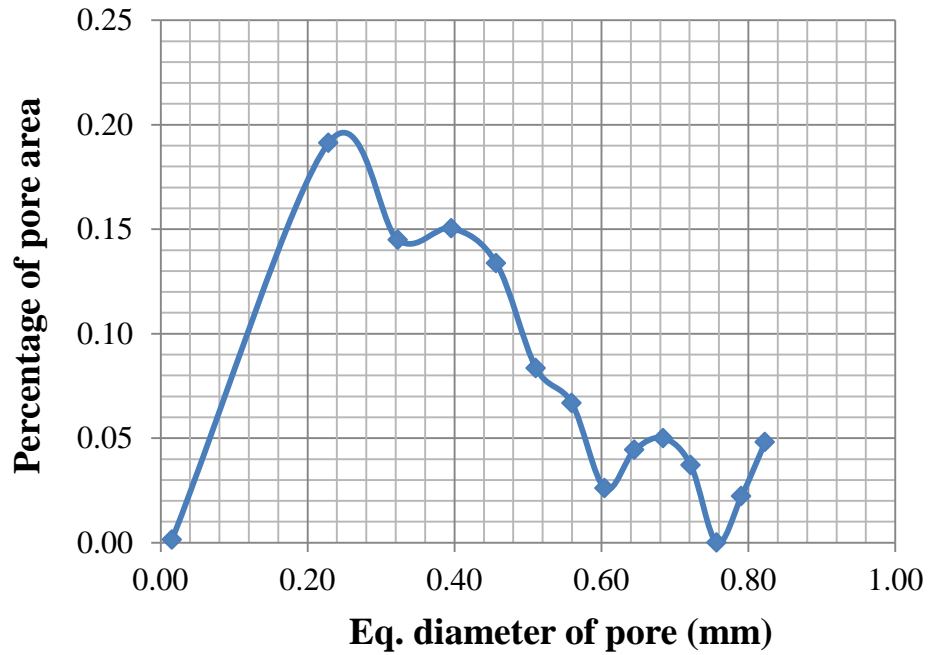
Fig. 5.1e Pore size distribution of sand in Image J
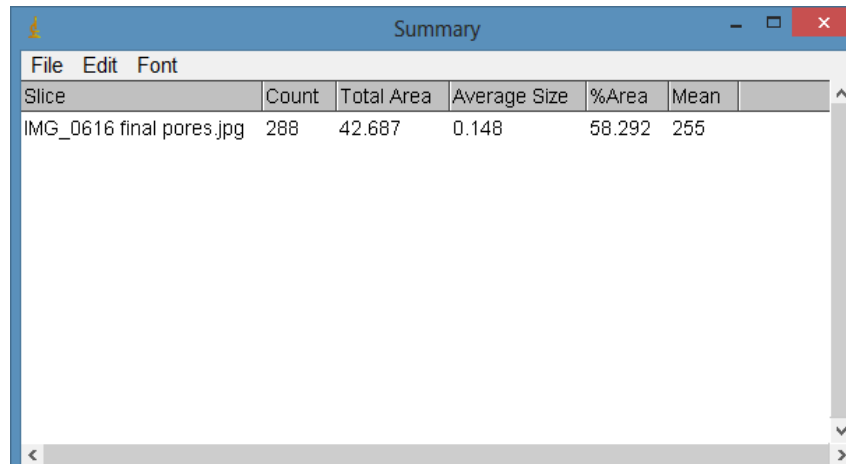
Fig. 5.1f Percentage of particle area (58.29%) of sand in Image J

	Image	Area	NbPixels	Density
Mean	--	31.8918	164040	0.421757
Min	--	31.8918	164040	0.421757
Max	--	31.8918	164040	0.421757

Fig. 5.1g Porosity of sand is 42.17 % in Avizo
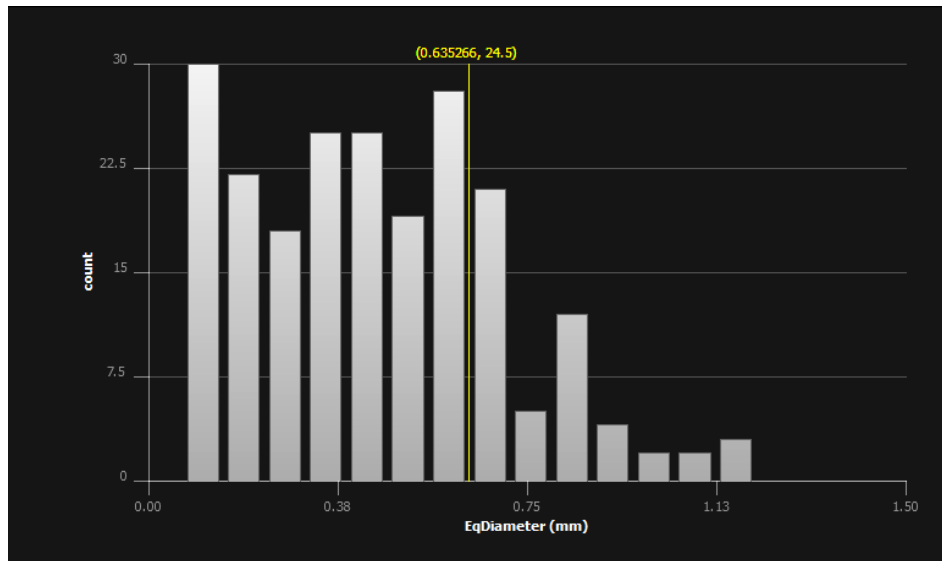
Fig. 5.1h Histogram of eq. diameter of particle in Avizo
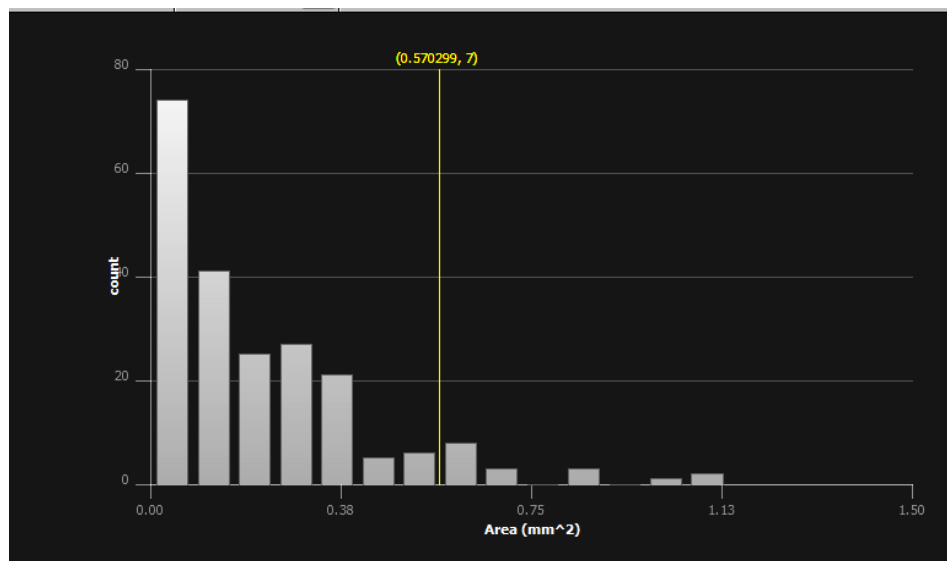
Fig. 5.1i Histogram of particle area in Avizo

	EqDiameter (mm)	Area (mm^2)
Mean	0.451945	0.210656
Min	0.0667507	0.00349946
Max	1.20265	1.13597
Median	0.436125	0.149801
Variance	0.063962	0.0455914

Fig. 5.1j Mean Eq. diameter is 0.45 mm and mean area of particles is 0.21 mm^2 in Avizo
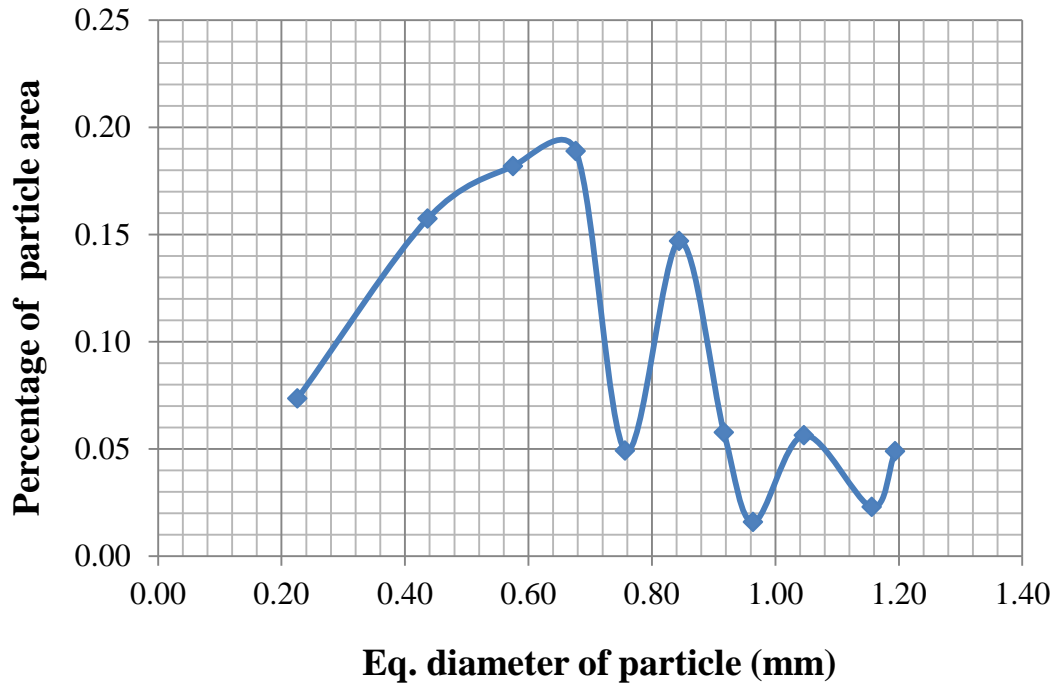
Fig. 5.1k Particle size distribution in Avizo

5.2 HYDRAULIC CONDUCTIVITY EXPERIMENT

Table 5.2a Time required to cause different head drop for 2.36 mm glass beads

Number of Measurements	Time (Seconds)		
	Under head difference of		
	300 mm	500 mm	700 mm
1	9.38	17.47	26.67
2	10.38	18.18	27.19
3	10.31	18.1	27.03
4	9.83	18.69	28.82
5	11.48	19.86	30
6	10.17	17.91	26.4
7	10.2	17.73	26.64
8	10.77	19.07	28.8
9	10.49	18.41	28.03

Average time (seconds)	**10.33**	**18.38**	**27.73**
k (m/s)	5.82×10^{-4}	6.36×10^{-4}	7.32×10^{-4}
$k_{avg}(m/s)$	**6.50×10^{-4}**

Table 5.2b Time required to cause different head drop for 3.075 mm glass beads

Number of Measurements	Time (Seconds)		
	Under head difference of		
	300 mm	500 mm	700 mm
1	9.72	16.94	24.43
2	9.58	16.56	24.35
3	9.29	16.32	24.21
4	10.12	17.57	26.1
5	9.14	15.94	23.73
6	9.14	15.89	23.77
7	9.42	16.24	24.03
8	9.21	16.08	23.73
9	9.07	15.86	23.49
Average time	9.41	16.38	24.20
k (m/s)	6.39×10^{-4}	7.13×10^{-4}	8.38×10^{-4}
$k_{avg}(m/s)$	**7.30×10^{-4}**

Table 5.2c Time required to cause different head drop for 3.6 mm glass beads

Number of Measurements	Time (Seconds)		
	Under head difference of		
	300 mm	500 mm	700 mm
1	8.72	15.35	23.04
2	9.11	15.96	24.01
3	9	15.85	23.77
4	8.81	15.4	22.86

5	9.18	16.07	24.14
6	9.12	15.6	23.26
7	9.23	16.15	24.29
8	8.9	15.5	23.02
9	8.87	15.54	23.47
Average time	8.99	15.71	23.54
k (m/s)	6.69×10^{-4}	7.43×10^{-4}	8.62×10^{-4}
$k_{avg}(m/s)$	7.58×10^{-4}		
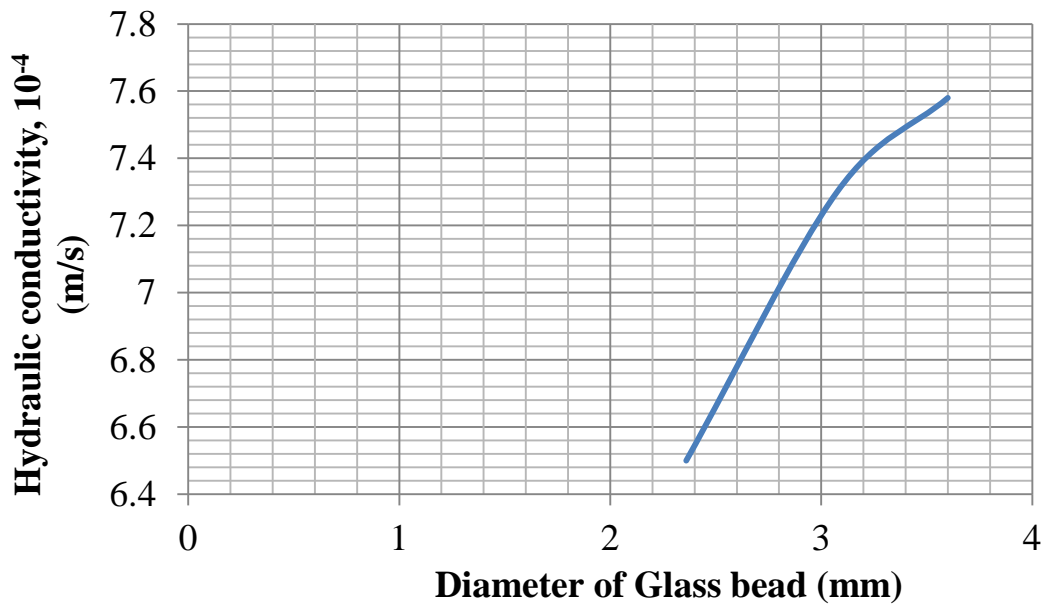
Fig. 5.2 Hydraulic conductivity versus diameter of glass bead

5.3 AIR PERMEABILITY EXEEPRIMENT

Table 5.3a Average of Air permeability for 0.46 mm glass beads

0.46 mm	Trial 1	Trial 2	Trial 3	AverageK (m^2)
200 lph	1.996E-11	1.882E-11	1.943E-11	1.940E-11
300 lph	2.136E-11	2.085E-11	2.085E-11	2.102E-11
500 lph	2.082E-11	2.085E-11	2.186E-11	2.118E-11
			Average K	2.05E-11

Table 5.3b Average of Air permeability for 1.29 mm glass beads

1.29 mm	Trial 1	Trial 2	Trial 3	AverageK (m^2)
200 lph	2.597E-11	2.596E-11	2.546E-11	2.580E-11
300 lph	2.762E-11	2.851E-11	2.824E-11	2.813E-11
500 lph	2.566E-11	2.600E-11	2.488E-11	2.551E-11
			Average K	*2.65E-11*

Table 5.3c Average of Air permeability for 2.36 mm glass beads

2.36 mm	Trial 1	Trial 2	Trial 3	AverageK (m^2)
200 lph	2.774E-11	2.748E-11	2.921E-11	2.814E-11
300 lph	3.069E-11	3.008E-11	3.043E-11	3.040E-11
500 lph	2.735E-11	2.680E-11	2.750E-11	2.722E-11
			Average K	*2.86E-11*

Table 5.3d Average of Air permeability for 3.075 mm glass beads

3.075 mm	Trial 1	Trial 2	Trial 3	AverageK (m^2)
200 lph	3.094E-11	3.039E-11	2.850E-11	2.994E-11
300 lph	2.811E-11	2.897E-11	3.009E-11	2.906E-11
500 lph	3.030E-11	3.036E-11	2.779E-11	2.948E-11
			Average K	*2.95E-11*

Table 5.3e Average of Air permeability for 3.6 mm glass beads

3.6 mm	Trial 1	Trial 2	Trial 3	AverageK (m^2)
200 lph	2.8670E-11	2.8780E-11	2.9250E-11	2.8900E-11
300 lph	3.0920E-11	3.2240E-11	3.1000E-11	3.1387E-11
500 lph	2.8620E-11	2.9210E-11	2.9450E-11	2.9093E-11
			Average K	*2.98E-11*

Table 5.3f Relationship between hydraulic conductivity and air permeability

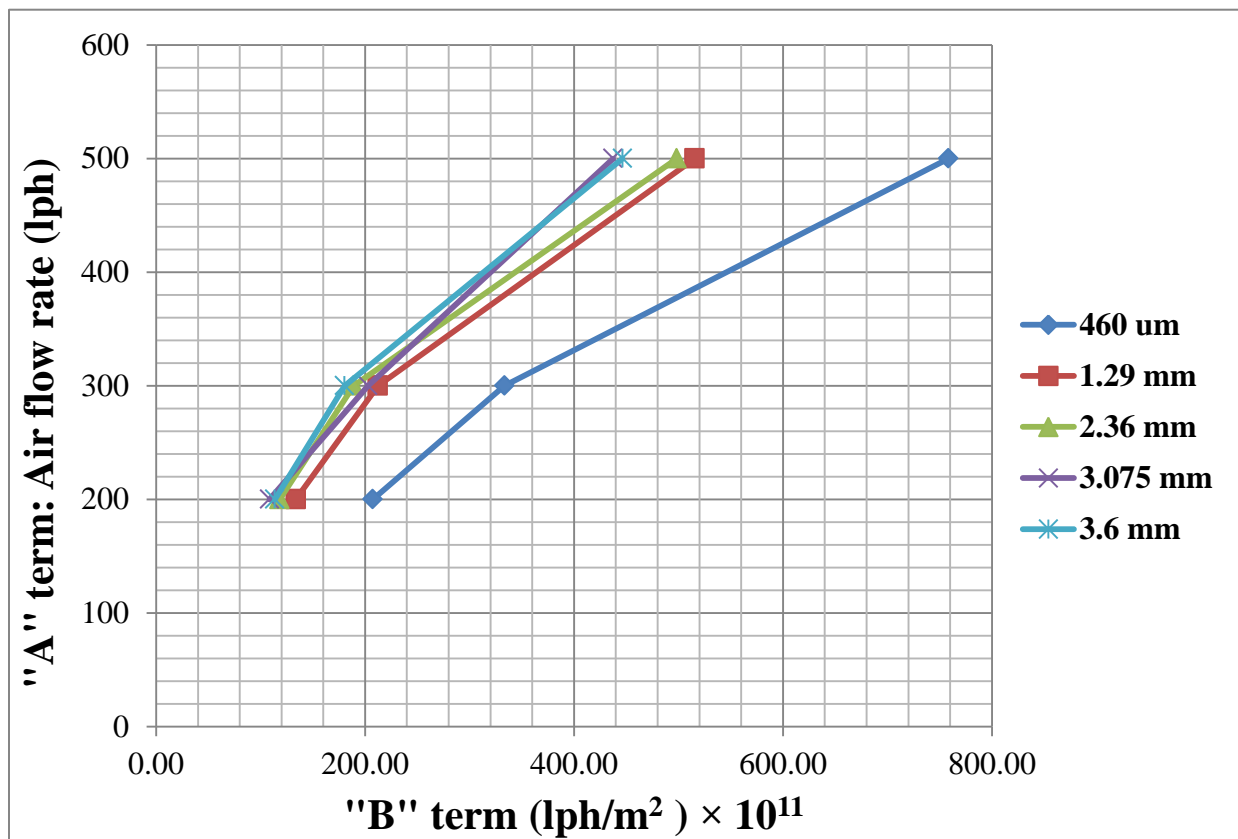| Diameter of glass bead (mm)	Air permeability ($\times 10^{-11}\,\mathrm{m}^2$)	Hydraulic conductivity($\times 10^{-4}$m/s)
3.6	2.98	2.92
3.075	2.95	2.89
2.36	2.86	2.80
1.29	2.65	2.60
0.46	2.05	2.01

Fig. 5.3a Graphical air permeability results for glass beads, where A term is Q and B term

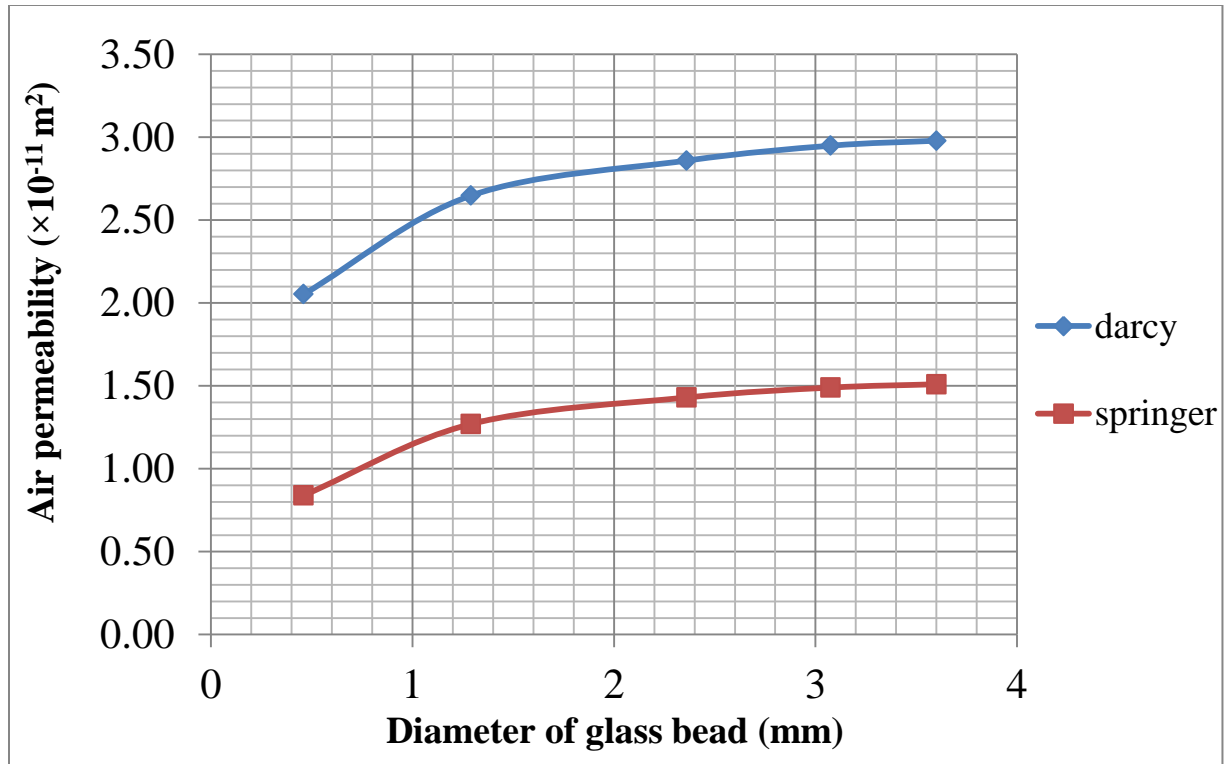is $[2 \times \mu \times L \times P_0 / A \times (P_0^2 - P_1^2)]^{-1}$

Fig. 5.3b Air permeability versus diameter of glass bead (mm)

5.4 DISCUSSIONS

Image analysis

Using the resin impregnated samples and image processing technique mentioned above the porosity, pore size distribution, pore area versus pore count and particle size distribution were obtained with the help of Image J and Avizo fire software and the same is presented in the form of Figs. 5.1a to 5.1f.

In Image J, the total porosity of the specimen prepared using Grade II sand is 40.59% from the Fig. 5.1b. The total particle area is observed to be 58.59% as shown in Fig. 5.1f. It was calculated that the total percentage of particle and pore area add to 99.18%. It was analysed that it is due to watershed segmentation tool used in Image J. Watershed segmentation creates thin lines which Image J includes in its analysis.

In Image J, the particle size distribution follows a normal distribution with a peak at 0.50 mm as Eq. diameter as shown in Fig. 5.1d. This means that maximum portion of image of sand

64

specimen shows particles with 0.50 mm as Eq. diameter. Another important observation was that in Image J, particle size distribution shows particles which are less than 0.10 mm. Such small particles occupy ~ 7% of the total particle area. It is also seen that instead of actual particles these can be small blemishes which has to be compulsorily removed. The tools of remove outliers here is seen to not completely eliminate the small spots. Hence, remove outliers tools is disadvantage in Image J and has to be carefully used. In Image J, it was observed that remove outliers tool which is used to eliminate small bright and dark particles should be used the minimum. It has a large effect on the shape and size of particle/pores if used a large number of times. It is recommended that it should be used less than 5 number of times. The pore size distribution has several peaks which shows different types of pore sizes are presentin Fig. 5.1e. Pore size distribution shows a peak at 0.25 mm which is less than particle size distribution peak of 0.50 mm. The advantage of Image J was that it provided particle area distribution and pore area distribution corresponding to a particular area. This area was converted into equivalent diameter by assuming an equivalent circular shape in Microsoft Excel. Thus, area distribution in terms of Eq. diameter can be evaluated. But the disadvantage is that the Image J doesnot provide equivalent diameter result.

There were large number of similarities in both the image processing softwares including that they help in plotting the histograms and size distribution. The particle size distribution from both the softwares shows similar curves. The porosity of the both the softwareshows a similar value.In both, the results which can be generated are porosity, particle area, particle count, pore area and pore count. Both helps in generation of area of particle and pore. An advantage in both was that size distribution of particles and pores can be evaluated simultaneously by changing the background of the thresholded image.

In Avizo fire, particle and pore size were provided both in the terms of area and equivalent diameter. Hence, it helps in saving the time to calculate equivalent diameter from area. Avizo had better tools in removing small spots as it had a negligible effect on the shape and size of particles. In Avizo fire, it was observed that the particle area is also included in the pore area as shown in Fig.4.1u when the watershed segmentation (separation) is performed. Hence, pore area is shown much greater value than actual pore area as shown by pore lines. Hence, Avizo fire is

not able to give correct pore size distribution results. Hence, it can be concluded that Image J is giving better results of pore size distribution as compared to Avizo fire.

Hydraulic conductivity

Using the methodology presented and the developed experimental setup, the hydraulic conductivity of different size glass beads has been obtained and the same is presented in Tables 5.2a, 5.2b and 5.2c. It can be observed that the values of hydraulic conductivity for 2.36 mm, 3.075 mm and 3.6 mm glass beads can be validated with theoretical hydraulic conductivity of sand. Further using the results presented in Tables 5.2a, 5.2b and 5.2c, the variation of hydraulic conductivity values of different glass beads with their size fraction has been plotted in the form of Fig. 5.2. It can be observed that experimentally obtained permeability values are in line with the usual range of permeability values as shown in Table 2.3b by Bear, 1972. The hydraulic conductivity values are valid to the experimental values as well as to the values shown by C.W. Fetter, 1994 because the magnitude of hydraulic conductivity is 10^{-4} m/s.

Air permeability

The results obtained from the air permeability experimental setup are shown in Tables 5.3a to 5.3e. Fig. 5.3a shows the graphical representation of the "A" term: air flow rate and "B" term: $[2 \times \mu \times L \times P_0 / A \times (P_0^2 - P_1^2)]^{-1}$ for glass beads and the slope of the best-fit line gives the air permeability. Air permeability values obtained are consistent with various trials and flow rates for any given size of glass bead. Air permeability values were plotted for two different equations Darcy and Springer equation and are shown in Fig. 5.3b. It can be seen that the air permeability decreases as the size of glass beads decreases. In conventional air permeability method, manometer was used for measurement of air pressure. Also, then the readings had to be taken manually. The automation of the air permeability method using digital pressure sensor, air flow meter and data logger gave good results. This method of air permeability is better because of lower deviation, less manual errors and more data collection. Another way of finding the hydraulic conductivity is from air permeability values, which were related as shown in Table 5.3f. Thus, the relationship between air permeability and hydraulic conductivity for glass beads was validated.

CHAPTER 6

CONCLUDING REMARKS

6.1 CONCLUSIONS

The resin impregnated methodology was successfully implemented in sand samples. DSLR camera was used for high quality image acquisition. Further, two image processing softwares Image J and Avizo fire were used for image processing and analysis successfully. Porosity, particle size distribution and pore size distribution of sand were evaluated with the help of these softwares. The results from the two softwares were compared in order to conclude a better software in terms of user friendly and results. The design and development of experimental test apparatus were taken up and completed as planned. With the help of this developed apparatus, air and water permeability were determined by conducting experiments on glass beads. The results obtained from permeability were validated with those available in the literature for the similar material tested. It was observed that since air permeability experiment was conducted using digital pressure sensor and high precision data logger, the permeability values were found to be consistent as compared to conventional methodologies.

In the research conducted following conclusion were arrived at:

- The low viscosity resin impregnation was successfully implemented in sand samples. The low viscosity resin helps in creation of smooth surfaces in order to minimize the amount of image corrections required during image processing.
- The colour dying of low viscosity resin showed good colour contrast hence, a better option than using low viscosity resin without colour dye. The requirement of polishing the surface is eliminated.
- Remove outliers tools of Image J has to be used minimum so that the shape and size of particles do not distort.
- Image J is more user-friendly and has good image segmentation, hence provides better pore size distribution results.
- Avizo fire has better morphological operations but poor image segmentation.
- A innovative method of air permeability based on Darcy's law with the help of digital pressure sensor and data logger was developed. Air permeability method as compared to

hydraulic conductivity showed better results because of lower deviation, less manual errors and more data collection.

- The relationship developed between hydraulic conductivity and air permeability was validated with the experimental values.

- It has been also seen that the applications of lightweight cellular cemented are wide in different types of structures in geo-environment. It was also concluded that resin impregnation technique is not possible in lightweight cellular cemented clay because of the presence of isolated air bubbles

6.2 SCOPE FOR FUTURE WORK

- Resin impregnation techniques can be tested on clay with the help of low viscosity resin.

- The application of proposed methodology for LWCCC should be tested as PRBs, low-densitymaterial and high strength material.

REFERENCES

1. ASTM D 5084-10 (2010). "Standard Test Methods for Measurement of Hydraulic Conductivity of Saturated Porous Materials Using a Flexible Wall Permeameter", *ASTM International*, West Conshohocken, PA.

2. ASTM D 5550-14 (2014). "Standard Test Method for Specific Gravity of Soil Solids by Gas Pycnometer", *ASTM International*, West Conshohocken, PA.

3. Bear, J. (1972). "*Dynamics of Fluids in Porous Media"*, American Elsevier, New York.

4. Blowes, D., Ptacek, C., Cherry, J., Gillham, R., and Robertson, W. (1995). "Passive Remediation of Groundwater Using In Situ Treatment Curtains," *Geoenvironment 2000: Characterization, Containment, Remediation, and Performance in Environmental Geotechnics,* American Society of Civil Engineers, Restov, VA, Geotechnical special publication, 46 (2), 1588-1607.

5. Cantrell, K., Martin, P., and Szecsody, J. (1994). "Clinoptilolite as an In Situ Permeable Barrier to Strontium Migration in Ground Water", *Thirty- Third Hanford Symposium on Health and the Environment, Part 2*, 839-850.

6. Carman, P.C. (1939). "Permeability of saturated sands, soils and clays",*Journal Agricultural Science,* 29(2), 263–73

7. Carmen, P. C. (1937). "Fluid Flow through Granular Bed", *Transaction of Institute of Chemical Engineers (London)*, 15, 150-156

8. Carmen, P.C. (1956), *"Flow of gases through porous media"*, Academic press, New York.

9. Cera-Chem Private Limited (2014). *"Ceraplast-AER, Air entraining admixtures"*, Datasheet, Chennai, India.

10. Czupak, Z.D. (2011). "Stabilization and imaging of cohesionless soil specimens", *Master Thesis,* Arizona State University, U.S.A.

11. Diamond, S. (1970). "Pore-size distribution in clays", *Clays and Clay Minerals*, 18, 7-23.

12. Doktor, T., Kytýř, D., Valach, J. and Jirošek, O. (2010). "Assessment of pore-size distribution using image analysis", *9th Youth Symposium on Experimental Solid Mechanics*, 155-157.

13. Doktor, T., Kytýř, D., Valach, J., Jirošek, O. and Kosteleckà, M. (2011). "Improvements of an analysis tool for the pore-size distribution assessment", *10th Youth Symposium on Experimental Solid Mechanics*, 45-46.

14. Elliot, T., R. and Heck, R., J. (2007). "A comparison of optical and X-ray CT technique for void analysis in soil thin section", *Geoderma,* 141 (1-2), 60-70.

15. Golder Associates Ltd. (1998). "*Active Containment: Combined Treatment and Containment Systems*", Department of the Environment, Transport and the Regions, London, ISBN 185112 114 5.

16. Graton, L. C., and Fraser, H. J (1935). "Systematic packing of spheres with particular relation to porosity and permeability", *Journal of Geology,* 43(8), 785-909.

17. Green, W.R. and Ampt, G.A. (1911). "Studies of soil physics. I. The flow of air and water through soils", *Journal of Agricultural Science*, 4(1), 1-24.

18. Hazen, A. (1892). "Some Physical Properties of Sands and Gravels with Special Reference to their Use in Filtration", *The 24th Annual Report of the State Board of Health of Massachusetts. Public Document No.34*, 539-556.

19. Horpibulsuk, S., Miura, N. and Nagaraj, T. S. (2003). "Assessment of strength development in cement-admixed high water content clays with Abrams' law as a basis", *Geotechnique*, 53(4), 439-444

20. Horpibulsuk, S., Phojan, W., Suddeepong, A. and Chinkulkijniwat, A. and Liu, M.D. (2012). "Strength development in blended cement admixed saline clay", *Applied Clay Science*, 55, 44-52.

21. Huntsman International Pvt. Ltd. (2012). *"Buildings blocks selectors guide for formulator"*, Advanced Materials: Raise performance with building blocks, Datasheet.

22. Indraratna, B., Pathirage, P., Rowe, K. and Banasiak L. (2014). "Coupled hydro-geochemical modeling of a permeable reactive barrier for treating acidic groundwater". *Computers and Geotechnics*, 55, 429-439.

23. IS 1498-2007. "*Classification and Identification of soils for general engineering purposes"*, Bureau of Indian Standards, New Delhi.

24. Jang, D. J., Frost, J.D. and J.Y. Park (1999). "Preparation of epoxy impregnated sand coupons for image analysis", *Geotechnical Testing Journal*, 22 (2), 147-158.

25. Kanagalakshmi, A.S., Latha, A., Ganesan, Jayashree, V. and Caroline Saro, J. (2015). "Experimental Analysis on Improving Concrete Quality by Using – SF Micro Silica", *International Journal of Scientific & Engineering Research*, 6(1), 414-419.

26. Kovács, G. (1981). "*Seepage hydraulics"*, Elsevier Scientific Pub. Co., Amsterdam.

27. Krumbein, W. C., Monk, G. D. (1942). "Permeability as a function of the size parameters of unconsolidated sand", *American Institute of Mining and Engineering*, Lttleton, CO. Tech. Pub., 151(1), 153-163.

28. Lawrence, G. P. (2006). "Measurement of pore sizes in fine-textured soils: A review of existing techniques", *Journal of Soil Science*, 28(4), 527-540.

29. Meyer, K. and Klobes, P.(1999). "Comparison between different presentations of pore size distribution in porous materials", *Fresenius Journal of Analytical Chemistry*, 363(2), 174-178.

30. Miki, H., Mori, M. and Chida, S. (2003). "Trial Embankment on soft ground using lightweight-foam mixed in-situ surface soil", *22nd PIARC World Road Congress*, Durban.

31. Nimmo, J.R., (2004). "Porosity and Pore Size Distribution", *Encyclopedia of Soils in the Environment*, 3, 295-303.

32. Oh, K. S. and Kim, T. H. (2013). "Evaluation of the effect of induced vibration on early age lightweight air-trapped soil", *International Journal of Civil Engineering*, 11(2 B), 141-149.

33. Richard long, P., Kenneth Demars, R., Raafat Mankbadi, R. and Alvaro Covo (1998). "The relationship between permeability coefficients for soil obtained using liquid and gas", *University of Connecticut Project*, U.S.A, 88-180.

34. Rozenbaum, O., Bruand, A. and Le Trong, E. (2012). "Soil porosity resulting from the assemblage of silt grains with a clay phase: New perspectives related to utilization of X-ray synchrotron computed microtomography, "*Comptes Rendus Geoscience*, 344(10), 516-525

35. Sardini, P., El Albani, A., Pret, D., Gaboreau, S., Siitari-Kauppi, M., and D. Beaufort (2009). "Mapping and quantifying the clay aggregate microporosity in medium-to coarse-grained sandstones using the 14C-PMMA method", *Journal of Sedimentary Research*, 79(8), 584-592.

36. Satoh, T., Tsuchida, T., Mitsukuri, K. and Hong, Z. (2001). "Field placing test of lightweight treated soil under seawater in Kumamoto port", *Japanese Geotechnical Society*, 41(5),145-154.

37. Springer, D. A. (1993). "Determining the air permeability of porous materials as a function of a variable water content under controlled laboratory conditions", *M.A. thesis*, Dept. of Geography, University of California, Santa Barbara, California, U.S.A.

38. Taylor, D. (1948). *"Fundamentals of Soil mechanics"*, John Wiley & Sons, Inc., New York.

39. Tratnyk, P., Johnson, T., Scherer, M., and Eykholt, G. (1997). "Remediating Groundwater with Zero-Valent Metals: Chemical Considerations in Barrier Design",*Ground Water Monitoring and Remediation*, 17(4), 108-114.

40. United States of America. Environmental Protection Agency. Office of Solid Waste and Emergency Response (U.S. EPA) (2012). *"A Citizen's Guide to Soil Vapor Extraction and Air Sparging"*, Environmental Protection Agency.

41. United States of America. Environmental Protection Agency .Office of Solid Waste and Emergency Response (U.S. EPA)(2001). *"A Citizen's Guide to Permeable Reactive Barriers, Environmental Protection Agency"*, Environmental Protection Agency.